



Akkermansia muciniphila secretes a glucagon-like peptide-1-inducing protein that improves glucose homeostasis and ameliorates metabolic disease in mice

Hyo Shin Yoon^{1,9}, Chung Hwan Cho^{1,9}, Myeong Sik Yun¹, Sung Jae Jang¹, Hyun Ju You^{1,2,3,4}, Jun-hyeong Kim⁵, Dohyun Han⁶, Kwang Hyun Cha⁷, Sung Hyun Moon^{1,5}, Kiuk Lee⁵, Yeon-Ji Kim⁸, Sung-Joon Lee⁸, Tae-Wook Nam⁵ and GwangPyo Ko^{1,3,4,5}✉

The gut microbiota, which includes *Akkermansia muciniphila*, is known to modulate energy metabolism, glucose tolerance, immune system maturation and function in humans^{1–4}. Although *A. muciniphila* is correlated with metabolic diseases and its beneficial causal effects were reported on host metabolism^{5–8}, the molecular mechanisms involved have not been identified. Here, we report that *A. muciniphila* increases thermogenesis and glucagon-like peptide-1 (GLP-1) secretion in high-fat-diet (HFD)-induced C57BL/6J mice by induction of uncoupling protein 1 in brown adipose tissue and systemic GLP-1 secretion. We apply fast protein liquid chromatography and liquid chromatography coupled to mass spectrophotometry analysis to identify an 84 kDa protein, named P9, that is secreted by *A. muciniphila*. Using L cells and mice fed on an HFD, we show that purified P9 alone is sufficient to induce GLP-1 secretion and brown adipose tissue thermogenesis. Using ligand-receptor capture analysis, we find that P9 interacts with intercellular adhesion molecule 2 (ICAM-2). Interleukin-6 deficiency abrogates the effects of P9 in glucose homeostasis and downregulates ICAM-2 expression. Our results show that the interactions between P9 and ICAM-2 could be targeted by therapeutics for metabolic diseases.

The prevalence of metabolic disease has reached epidemic proportions during the past three decades⁹. The human gut microbiota regulates various metabolic functions, including intestinal barrier homeostasis, glucose homeostasis and energy absorption^{1–4}. Several studies have demonstrated that an abundance of *A. muciniphila* is correlated with metabolic disorders, such as obesity and type-2 diabetes, in both preclinical and clinical studies^{10–15}, and that supplementation with viable or pasteurized *A. muciniphila* ameliorates metabolic endotoxemia and improves gut-barrier function, thereby improving the systemic metabolic profile^{3–8}. Furthermore, the presence of *A. muciniphila* reduces the intestinal energy absorptive capacity under cold conditions² and the presence of *A. muciniphila* is correlated with fat browning^{16,17}. Moreover, pasteurized

A. muciniphila has direct effects on the host energy expenditure¹⁸. Little evidence for the mechanisms involved, including specific host cellular components or bacterial proteins, in the beneficial effects of *A. muciniphila* has been reported. In particular, investigation of the relationship between *A. muciniphila* and host adipose tissue depots—including interscapular brown adipose tissue (iBAT), which mediates non-shivering thermogenesis—is lacking.

The gut microbiota is known to influence the enteroendocrine system^{19,20} and modulate the host immune system through microbially derived metabolites or cellular membrane components²¹. In particular, bacterial metabolites, such as short-chain fatty acids (SCFAs)^{22–26}, secondary bile acids^{27–29}, indoles³⁰ and lipopolysaccharide³¹, regulate appetite by stimulating the release of gut hormones, such as GLP-1, and by activating enteric neuronal signalling³², which contribute to energy homeostasis. The bacterial chaperone protein ClpB, which is present in commensal and pathogenic bacteria, has been shown to regulate appetite³³. Although it is known that *A. muciniphila* affects the gut-hormone-releasing L cells in the gut³⁴, evidence of the bioactive molecule of *A. muciniphila* that is involved in GLP-1 secretion is lacking.

Gut-microbiota-associated proteins also activate the host immune system³⁵. Recent research suggests that, in contrast to other commensal bacteria³⁶, *A. muciniphila* induces a unique type of immune response that involves homeostatic antigen-specific-IgG antibody and T-cell responses, and a cytotoxic T-cell response in a colorectal cancer model^{21,37}. Furthermore, in high-fat-diet (HFD)-fed mice, this bacterium activates adipose-tissue-resident regulatory T-cells, and its component, Amuc_1100, has been reported to interact with toll-like receptor 2 (refs. 7,38).

As reported previously^{5,7}, oral administration of *A. muciniphila* (ATCC-BAA-835) significantly reduced body mass, improved glucose tolerance, and increased the serum concentrations of insulin and β -oxidation gene markers compared with HFD-fed mice (Extended Data Fig. 1a–g). Interestingly, the mass and size of the iBAT were lower, whereas the mass and size of the epididymal

¹Department of Environmental Health Sciences, Graduate School of Public Health, Seoul National University, Seoul, Korea. ²Institute of Health and Environment, Seoul National University, Seoul, Korea. ³Bio-MAX/N-Bio, Seoul National University, Seoul, Korea. ⁴Center for Human and Environmental Microbiome, Seoul National University, Seoul, Korea. ⁵KoBioLabs Inc., Seoul, Korea. ⁶Proteomics Core Facility, Biomedical Research Institute, Seoul National University Hospital, Seoul, Korea. ⁷Natural Product Informatics Research Center, Korea Institute of Science and Technology, Gangneung, Korea. ⁸Department of Biotechnology, College of Life Sciences and Biotechnology, School of Life Sciences and Biotechnology, Korea University, Seoul, Korea. ⁹These authors contributed equally: Hyo Shin Yoon, Chung Hwan Cho. ✉e-mail: gko@snu.ac.kr

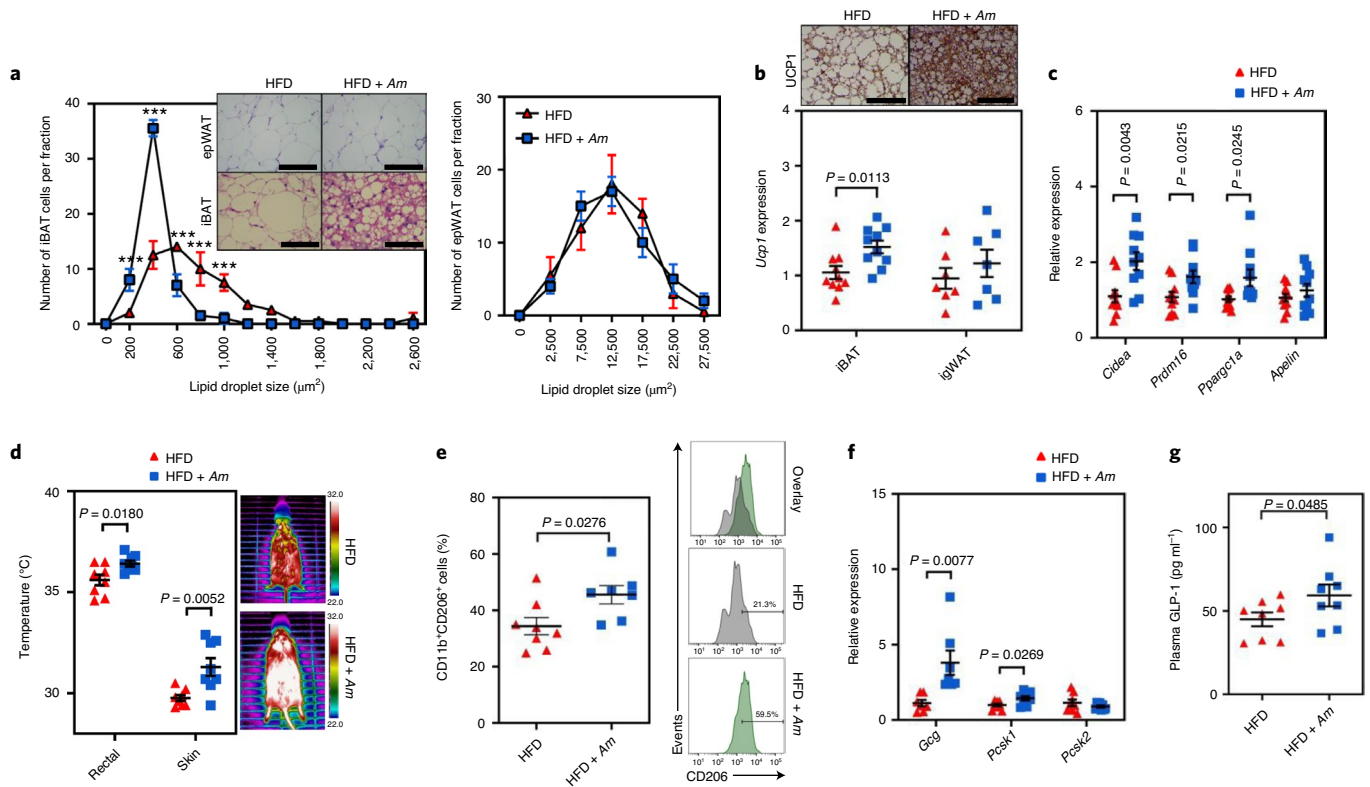


Fig. 1 | *A. muciniphila* activates brown adipocytes and induces GLP-1 expression. **a**, Frequency distribution of the surface area of the iBAT (left) and epWAT (right) after 14 weeks of consumption of an HFD, or an HFD supplemented with *A. muciniphila* (HFD + *A. muciniphila* (Am)). $n = 50$ cells were measured from three mice per group. Representative haematoxylin and eosin (H&E)-stained sections of epWAT (top) and iBAT (bottom). Scale bars, 100 μm . $n = 3$ per group. **b**, Representative immunohistochemical images of UCP1 expression (brown) in iBAT ($n = 3$ per group) and quantitative PCR with reverse transcription (RT-qPCR) analysis of *Ucp1* expression in iBAT and igWAT. Scale bars, 100 μm . **c**, Thermogenic iBAT-specific gene expression after *A. muciniphila* treatment. **d**, Rectal and dorsal skin temperatures (left). Right, dorsal temperature, measured using infrared thermography. **e**, Flow cytometry analysis of M2 macrophages in the stromal vascular fraction of the iBAT as a dot plot (left) and histogram (right). **f**, mRNA expression of *Gcg*, *Pcsk1* and *Pcsk2* in the ileum. **g**, Plasma GLP-1 concentration 10 min after oral glucose challenge. For **a–g**, data are mean \pm s.e.m. $n = 7–10$ (HFD) and $n = 7–10$ (HFD + *A. muciniphila*) mice per group. Statistical significance was calculated using two-tailed unpaired *t*-tests; *** $P < 0.001$.

white adipose tissue (epWAT) in HFD-fed mice were unaffected by *A. muciniphila* treatment (Fig. 1a and Extended Data Fig. 1c). These results are consistent with the recent findings that the administration of viable *A. muciniphila* does not affect epWAT adipocyte diameter or fat mass⁷, which suggests that there is a specific loss of iBAT after *A. muciniphila* treatment. Next, to assess the functional metabolic capacity of iBAT, we analysed thermogenic gene transcription. A significant induction of the mitochondrial-specific gene encoding uncoupling protein 1 (*Ucp1*) and the related thermogenic differentiation marker transcripts was observed in the iBAT (Fig. 1b,c) but not in the inguinal WAT (igWAT) of HFD-fed mice administered with *A. muciniphila* (Fig. 1b), which implies that the anti-obesogenic effects of *A. muciniphila* act through the iBAT, rather than the igWAT. Skin temperature over the iBAT as well as rectal temperature were significantly higher in HFD-fed mice administered with *A. muciniphila* compared with the controls (Fig. 1d). Furthermore, the number of anti-inflammatory M2 macrophages (CD11b⁺CD206⁺) in the iBAT was significantly higher in mice administered with *A. muciniphila* (Fig. 1e).

A. muciniphila and S24-7 (also known as Muribaculaceae) family spp. were more abundant in mice that were orally administered with *A. muciniphila* and, similarly, the 16S rRNA gene count for *A. muciniphila* was positively correlated with both iBAT temperature and plasma GLP-1 concentration, and negatively correlated with the level of glucose intolerance (Extended Data Fig. 2a–e). Moreover, transcripts of M2 macrophage markers were increased in the iBAT

of mice administered with *A. muciniphila* (Extended Data Fig. 2f–h). These results show that *A. muciniphila* influences the thermogenic activity of iBAT and the abundance of iBAT-specific M2-like macrophages in mice.

To evaluate the underlying mechanism of thermogenic gene upregulation in the iBAT, we compared the caecal metabolites between mice that were orally administered with viable *A. muciniphila* and control HFD-fed mice. Although creatine and glycine were present at higher concentrations in the caecal contents of treated mice compared with the controls, there were few differences. We therefore concluded that *A. muciniphila* treatment did not have a major impact on caecal metabolites (Extended Data Fig. 1h).

GLP-1 regulates BAT thermogenesis^{39–41}, so we next investigated whether oral administration of *A. muciniphila* affects GLP-1 expression in cultured L cells and in HFD-fed mice. As most GLP-1-secreting L cells are located in the distal ileum, we measured GLP-1 expression in the ileum after oral administration of *A. muciniphila* in HFD-fed mice. Transcription of *Gcg* (which encodes GLP-1 or glucagon), *Pcsk1* and *Pcsk2* was measured in each group of mice. A much higher expression of *Gcg* and *Pcsk1* was found in HFD-fed mice that were orally administered with *A. muciniphila* compared with the controls (Fig. 1f). Similarly, the plasma GLP-1 concentration was higher in HFD-fed mice that were orally administered with *A. muciniphila* compared with the controls (Fig. 1g).

Next, to identify how *A. muciniphila* induces GLP-1 secretion, we treated human enteroendocrine L cells (NCI-H716) with live

A. muciniphila (SNUG-61027, isolated from human faeces with ethical approval or ATCC-BAA-835) pellets or the culture supernatants of the bacteria, and then measured GLP-1 concentration. We found that the cell-free supernatant (CFS) substantially increased GLP-1 whereas the bacterial pellet did not (Extended Data Fig. 3a). To determine whether this effect was dose dependent, we treated NCI-H716 cells with *A. muciniphila* CFS at concentrations of 10–100% (v/v) and found that GLP-1 was induced in a dose-dependent manner (Extended Data Fig. 3b). We tested the effects of 23 *Lactobacillus* and 24 *Bifidobacterium* strains isolated from human faeces with ethical approval on GLP-1 secretion by NCI-H716 cells. The CFS (10% v/v) of ATCC-BAA-835 and of a newly isolated SNUG-61027 strongly induced GLP-1 secretion, whereas the CFS of all 47 strains tested had no effect (Extended Data Fig. 3c and Supplementary Table 1b).

As enteroendocrine cells can respond to SCFAs by increasing their secretion of GLP-1, acetate and propionate, which are present in the *A. muciniphila* CFS, were administered to enteroendocrine cells. However, although GLP-1 secretion was increased, it was not by as much as the increase that was observed in the CFS, suggesting that SCFAs are not the only bacterial products that induce GLP-1 secretion (Extended Data Fig. 3d,e).

To identify other *A. muciniphila*-derived molecule(s) that are responsible for the GLP-1 secretion, CFS of *A. muciniphila* (SNUG-61027) that was cultured in 5% fetal bovine serum (FBS)-based brain–heart infusion broth medium was filtered as described previously¹² to produce a series of fractions (Extended Data Fig. 4a). NCI-H716 cells were treated with 5 mg of each fraction and GLP-1 secretion was measured. Interestingly, the 100–300 kDa filtrate substantially increased GLP-1 secretion, and the 30–100 kDa filtrate increased GLP-1 secretion, but to a lesser extent (Extended Data Fig. 4b). Treatment with proteinase K abolished the effects of both fractions, indicating that the molecule or molecules responsible for the induction of GLP-1 secretion is probably a protein(s) (Extended Data Fig. 4c). To isolate the candidate protein(s) produced by *A. muciniphila*, the 100–300 kDa filtrate of SNUG-61027 and control medium, both of which contained approximately 25 mg ml⁻¹ protein, were passed through anion-exchange Mono Q columns, the collected fractions were used to treat NCI-H716 cells and the GLP-1 concentrations were measured. The m2–m4 fractions induced GLP-1 secretion (Extended Data Fig. 4d); these fractions were therefore concentrated and applied to size-exclusion columns to obtain further fractions, which were tested for their ability to induce GLP-1 secretion. Of these, the G17–G20 fractions induced the most GLP-1 secretion by L cells (Extended Data Fig. 4e).

Further analysis of these fractions was performed using liquid chromatography coupled with tandem mass spectrometry (LC–MS/MS) to identify the proteins that are responsible for GLP-1 secretion. Approximately 90 µg of protein from the 100–300 kDa filtrate obtained from the size cut-off filtration (sample 1), the products of ion-exchange chromatography (sample 2) and the products of the size-exclusion chromatography (sample 3) were analysed. Bovine-specific proteins that were present in the basal medium were excluded from the list of candidate proteins. Ninety-eight *A. muciniphila*-derived proteins and 130 bovine-specific proteins were identified: 95 in sample 1, 36 in sample 2 and 10 in sample 3 (Extended Data Fig. 4f), a list of which is provided in Supplementary Table 3. An overview of the proteins identified under each filtration condition, before and after filtering for proteins predicted to be secreted, is shown (Fig. 2a).

To investigate the effects of *A. muciniphila*-derived proteins, we cloned the cDNAs corresponding to the proteins identified in sample 3 (Methods), and each protein was tested for its ability to induce GLP-1 secretion in L cells. The outer membrane protein Amuc_1100—which is derived from ATCC-BAA-835 and has previously been shown to prevent obesity by restoring gut-barrier

integrity and increasing the secretion of endocannabinoid-like lipid molecules—was also expressed as a control, as in the previous study. We confirmed the production of a single protein of the correct size from each plasmid using SDS–polyacrylamide gel electrophoresis (Extended Data Fig. 4g). A list of the proteins identified in sample 3 is provided in Extended Data Fig. 4h and the sequence of each protein had a high similarity (>98%) to that of equivalent proteins produced by the type strain (ATCC-BAA-835).

We treated NCI-H716 cells with each of the nine proteins expressed, and P1 (UniProt: B2UKW8), P5 (UniProt: B2URM2) and P9 (UniProt: B2UM07) were shown to induce GLP-1 in a dose-dependent manner in NCI-H716 cells. However, the effect of Amuc_1100 in inducing GLP-1 secretion was negligible compared with the effect of P9 (Fig. 2b). GLP-1 induction by P9 was also confirmed in human primary intestinal epithelial cells (Fig. 2b). To determine whether these effects would also be present in mice that were fed a normal chow diet, mice were intraperitoneally (i.p.) injected daily with each protein for 2 weeks, and their weight gain and glucose tolerance were compared. Significant weight loss and a decrease in glucose intolerance were shown in mice that were treated with P9, in contrast to the effects of the other proteins (Extended Data Fig. 5a,b). Furthermore, to verify whether cloned proteins homologous to P9 that were derived from other gut bacteria have similar effects to P9, and because P9 belongs to the peptidase S41A family, we cloned the equivalent S41 member to P9 from *Escherichia coli* (*EcPrc*) and compared its ability to induce GLP-1 with that of P9 from *A. muciniphila* in NCI-H716 cells (Extended Data Fig. 5c). Interestingly, P9 from *A. muciniphila* induced GLP-1 but *EcPrc* did not in L cells, which indicates that *A. muciniphila*-derived P9 has a specific effect on GLP-1 secretion.

We also compared the effects of P9 on GLP-1 secretion with acetate and propionate in mice. A single i.p. injection of P9 induced a high level of GLP-1 secretion, whereas i.p. injection with SCFAs or *EcPrc* in mice did not, demonstrating that *A. muciniphila*-derived P9 induces GLP-1 through a different mechanism compared with the other GLP-1 inducers, such as SCFAs in vivo (Extended Data Fig. 5d).

Consistent results were also obtained in HFD-fed mice that were orally administered P9 daily for 8 weeks—mice that were fed P9 showed significantly lower weight gain (Fig. 2c) and food intake (Fig. 2d) compared with the controls. The adipose tissue volume (Fig. 2e,f and Extended Data Fig. 6a) and the glucose intolerance (Fig. 2g) of the mice were also significantly lower, whereas the ileal *Gcg* and *Pcsk1* expression was significantly higher (Fig. 2h). Furthermore, P9 induced thermogenesis, as shown by significant increases in the expression of BAT-specific genes (Fig. 2i) and in body temperature (Fig. 2j and Extended Data Fig. 6b) at room temperature and after a cold shock. Body composition analysis revealed significantly higher lean mass and lower fat mass (Extended Data Fig. 7a). Moreover, indirect calorimetry showed that mice that were administered with P9 had a lower respiratory quotient and higher fatty acid oxidation, although without any difference in energy expenditure (Extended Data Fig. 7b–d). Collectively, these results indicate that the administration of P9 prevents obesity by regulating glucose homeostasis and inducing thermogenesis by iBAT.

Next, to determine how P9 induces higher GLP-1 expression, RNA-sequencing (RNA-seq) analysis was performed in P9-treated NCI-H716 and control cells. Notably, P9 induced the expression of genes encoding calcium-related signalling proteins (Fig. 3a and Supplementary Table 7). Furthermore, using a phosphokinase array, we found that P9 increased the expression of phosphorylated cAMP-response-element-binding protein (p-CREB) and phosphorylated heat shock protein 27 (p-HSP27; Extended Data Fig. 8a). Calcium influx was significantly higher (Extended Data Fig. 8b), and pretreatment with calcium inhibitors reduced the P9-induced expression of GLP-1 (Fig. 3b and Extended Data Fig. 8c).

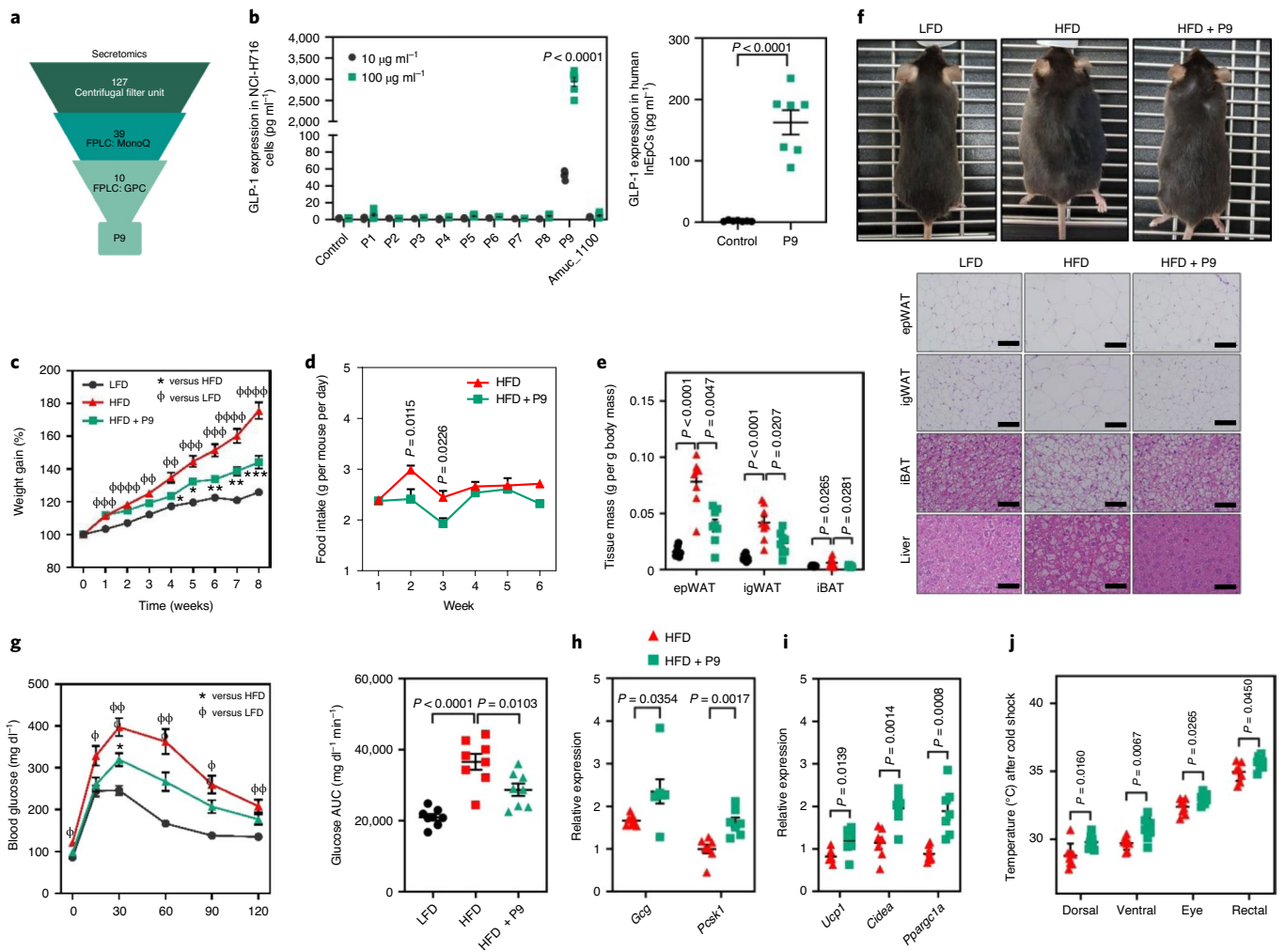


Fig. 2 | A purified GLP-1-inducing protein, P9, from *A. muciniphila* ameliorates obesity and influences glucose homeostasis by promoting thermogenesis.

a, Overview of the number of proteins identified following the various types of filtration, before and after filtering for proteins that were predicted to be secreted. FPLC, fast protein liquid chromatography; MonoQ, anion-exchange column chromatography; GPC, gel permeation chromatography. **b**, Expression of GLP-1 after treating NCI-H716 cells with purified proteins produced by *A. muciniphila* (data represent three independent experiments performed in duplicate, $n = 6$ per group; left) and treating human primary intestinal epithelial cells (IntEpCs) with P9 ($50 \mu\text{g ml}^{-1}$; $n = 7$ per group; right). **c**, Weight gain in HFD-fed mice that were orally administered with P9 ($100 \mu\text{g}$ per mouse) for 8 weeks. **d**, Food intake (g per mouse per day) (red, HFD; green, HFD + P9). **e**, Tissue masses (g per g body mass). **f**, The appearance of the mice (top) and H&E-stained sections of each adipose depot (bottom). Scale bars, $100 \mu\text{m}$. $n = 3$ per group. **g**, Oral glucose tolerance testing (left) was conducted, and the areas under the curves were measured (right). **h**, Expression of GLP-1-specific genes in the ileum. **i**, Expression of thermogenesis-specific genes in the iBAT. **j**, Temperatures of several parts of the body (dorsal, ventral, eye, rectal) after a cold shock at 5°C for 4 h. Data are mean \pm s.e.m. Number of mice per group: for **c–e**, **g–h** and **j**, low-fat diet: $n = 8$ (**c**, **e** and **g**), HFD: $n = 8$, HFD + P9: $n = 8$; for **i**, HFD: $n = 7$, HFD + P9: $n = 7$. Data were analysed using the Kruskal-Wallis test followed by Dunn's post hoc test, with comparison to the control group for **b** (left). For **c** and **d**, data were analysed using two-way analysis of variance (ANOVA), followed by the Bonferroni post hoc test; for **g** (left), two-way ANOVA, followed by Tukey's post hoc test; for **g** (right), one-way ANOVA, followed by Tukey's post hoc test. For **b** (right), **e** and **h–j**, statistical analysis was performed using two-tailed unpaired *t*-tests. The asterisks (*) and phi (Φ) indicate statistical significance; Φ or * $P < 0.05$, $\Phi\Phi$ or ** $P < 0.01$, $\Phi\Phi\Phi$ or *** $P < 0.001$, $\Phi\Phi\Phi\Phi$ or **** $P < 0.0001$.

A GLP-1 receptor β -arrestin assay confirmed that P9 does not bind to the GLP-1 receptor (Extended Data Fig. 8d). Moreover, pretreatment with inhibitors of G-protein-coupled receptor (GPCR) histamine H1 receptor, alpha-1 β adrenergic receptor and muscarinic acetylcholine receptor M1 did not alter GLP-1 secretion by L cells after P9 treatment (Extended Data Fig. 8e). To identify the receptor for P9, we performed a protein-binding assay using ligand-receptor capture (LRC)-TriCEPS technology. The cellular proteins that bound to P9 in NCI-H716 cells were identified using LC-MS/MS (Fig. 3c). The most significantly enriched P9-binding protein was kinectin 1 (KTN1), and the most

abundantly enriched protein was ICAM-2. We therefore pretreated cells with ICAM-2 peptide or anti-ICAM-2 or anti-KTN1 antibodies, and measured the P9-induced GLP-1 secretion. Interestingly, ICAM-2 peptide significantly reduced P9-induced GLP-1 secretion in a dose-dependent manner (Fig. 3d). Next, to determine the importance of the interaction with ICAM-2, we pretreated cells with anti-ICAM-2 antibodies and measured the effects of P9. GLP-1 secretion was significantly reduced by treating the cells in this manner; however, the level of suppression was insufficient to prevent the entire effect of ICAM-2 (Fig. 3e). These results indicate that P9 directly binds to ICAM-2.

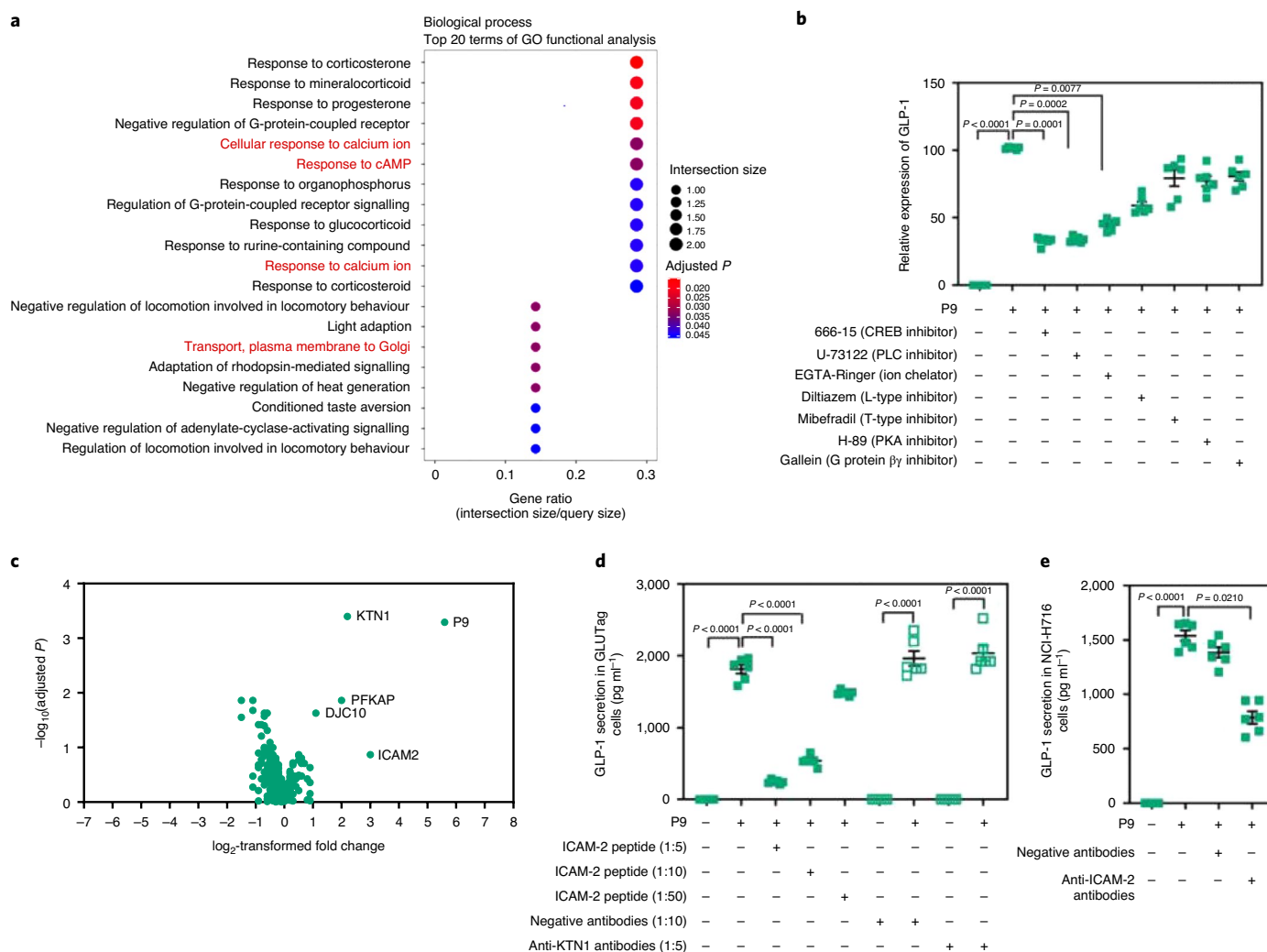


Fig. 3 | P9 induces GLP-1 secretion through a Ca^{2+} -dependent pathway and ICAM-2. **a, RNA-seq analysis of NCI-H716 cells treated with P9 ($50 \mu\text{g ml}^{-1}$) for 30 min. $n=3$ per group. **b**, GLP-1 secretion by GLUTag cells that were pretreated with calcium inhibitors ($10 \mu\text{M}$) for 15 min, and then with P9 ($100 \mu\text{g ml}^{-1}$) for 2 h. $n=6$ per group. **c**, An LRC-TriCEPS experiment (Dualsystems Biotech) using P9 was performed in NCI-H716 cells. $n=3$ per group. The enriched proteins were purified and processed for MS-based proteomics analysis (LC-MS/MS) and the *P* values obtained were adjusted for multiple testing using the Benjamini-Hochberg method. **d**, GLP-1 secretion was measured after treatment of GLUTag cells with ICAM-2 peptide (concentration of 1:5, 1:10 or 1:50) or anti-KTN1 antibodies (1:5) for 1 h and then with P9 ($50 \mu\text{g ml}^{-1}$) for 1 h. **e**, GLP-1 secretion was measured after treatment of NCI-H716 cells with anti-ICAM-2 antibodies (concentration of 1:10) for 1 h and then with P9 ($50 \mu\text{g ml}^{-1}$) for 1 h. **d, e**, $n=6$ per group. For **b, d** and **e**, data are mean \pm s.e.m. For **a**, correction for multiple testing was performed using the Benjamini-Hochberg method. For **b, d** and **e**, data represent the results of three independent experiments performed in duplicate. For **b** and **e**, data were analysed using the Kruskal-Wallis test followed by Dunn's post hoc test. For **d**, data were analysed using two-tailed unpaired *t*-tests.**

The increase in interleukin-6 (IL-6) secretion that is induced by exercise has been reported to stimulate GLP-1 secretion by intestinal L cells and pancreatic α -cells, thereby promoting insulin secretion⁴³. More recently, proinflammatory stimuli, such as endotoxin and IL-1 β , have been shown to induce GLP-1 secretion in an IL-6-dependent manner, causing a reduction in blood glucose⁴⁴. We therefore hypothesized that P9 may not only induce GLP-1, but also IL-6, which regulates glucose homeostasis. We found that P9 strongly induced IL-6 expression in macrophage cell lines (Extended Data Fig. 9a). We also found that *A. muciniphila* induced specific cytokine expression patterns, characterized by an upregulation of IL-6 but not tumour necrosis factor- α in the ileum and colon of HFD-fed mice, and in macrophages and colonic epithelial cells in vitro (Extended Data Fig. 11-n and Supplementary Table 1a). IL-6 increased thermogenic gene expression in immortalized brown preadipocytes (BACs; Extended Data Fig. 9b). Similarly,

Ucp1 expression was significantly increased by IL-6 treatment in primary preadipocytes that were obtained from HFD-fed mice (Extended Data Fig. 9c). IL-6 induces GLP-1 in GLUTag cells, although to a lesser extent compared with the P9-treated group, and the additive effects of GLP-1 secretion were observed after treatment with both P9 and IL-6 compared with the P9-treated group (Extended Data Fig. 9d,e).

To determine whether the effects of P9 on glucose tolerance and obesity require the GLP-1 receptor (GLP-1R) signalling pathway and whether these effects are IL-6 dependent, we i.p. injected exendin(9-39) (a GLP-1R antagonist) and orally administered P9 into HFD-fed mice, and compared the effects with the injection of P9 alone. Interestingly, exendin(9-39) treatment suppressed the effects of P9 on glucose tolerance (Fig. 4a), insulin tolerance (Extended Data Fig. 10c), weight gain and food intake (Extended Data Fig. 10d-e), which suggests that P9 activates the GLP-1 receptor pathway and

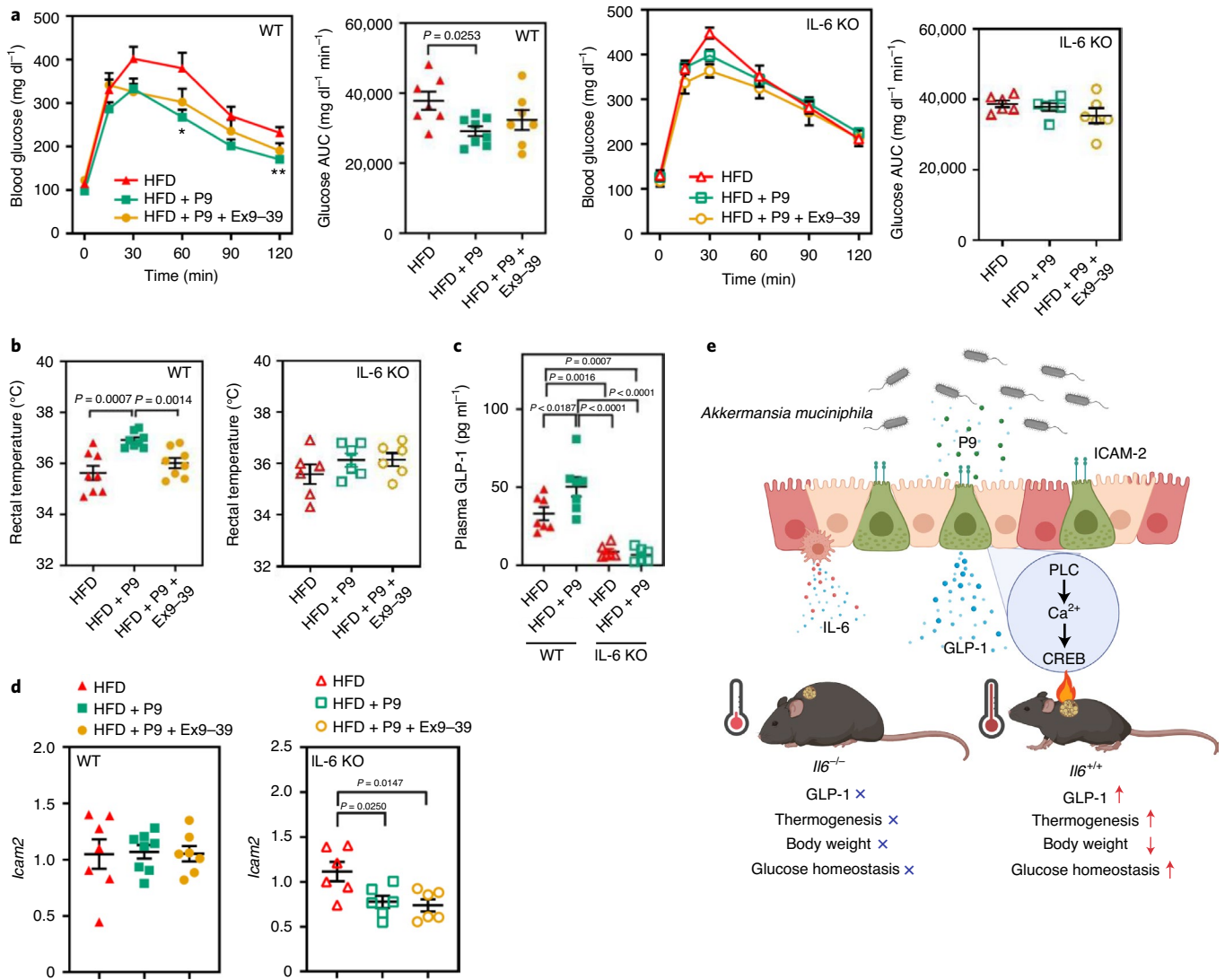


Fig. 4 | P9 regulates glucose homeostasis and promotes thermogenesis through the GLP-1R signalling pathway and IL-6. **a**, Oral glucose tolerance testing and area under the curve data for WT and IL-6-KO HFD-fed mice that were orally administered with P9 (100 μ g per mouse) with or without i.p. injection of exendin(9-39) (Ex9-39; GLP-1R antagonist; 0.8 μ g per mouse) for 8 weeks. **b**, Rectal temperatures of WT (left) and IL-6-KO (right) mice. **c**, Plasma GLP-1 concentration in WT and IL-6-KO mice. **d**, *Icam2* mRNA expression in the ileum of WT (left) and IL-6-KO (right) mice. **e**, Summary of the identified mechanism. The figure was created using BioRender.com. For **a-d**, data are mean \pm s.e.m. Number of mice per group: for **a** and **b**, WT: $n = 7$ (HFD), $n = 7$ (HFD + P9), $n = 7$ (HFD + P9 + exendin(9-39)); IL-6 KO: $n = 6$ (HFD), $n = 6$ (HFD + P9), $n = 6$ (HFD + P9 + exendin(9-39)); for **c** and **d**, WT: $n = 7$ (HFD), $n = 8$ (HFD + P9), $n = 7$ (HFD + P9 + exendin(9-39)); IL-6 KO: $n = 6$ (HFD), $n = 6$ (HFD + P9), $n = 6$ (HFD + P9 + exendin(9-39)). Data were analysed using two-way ANOVA followed by Tukey's post hoc test (**a**); one-way ANOVA followed by Tukey's post hoc test (**b-c**); and two-tailed unpaired *t*-tests (**d**).

that this mediates its effects on glucose homeostasis and body mass. Interestingly, the effects of P9 on glucose homeostasis were completely abrogated in IL-6-knockout (KO) mice, which implies that IL-6 is essential for the induction of GLP-1 secretion by P9 and its effects on glucose homeostasis. Although P9 alone induced thermogenesis, the coinjection of exendin(9-39) was associated with a lower rectal temperature, both at room temperature and after cold shock. Moreover, these effects of P9 were not observed in IL-6-KO mice (Fig. 4b and Extended Data Fig. 10f), which suggests that both GLP-1R signalling and IL-6 are involved in iBAT activation and thermogenesis. The circulating GLP-1 concentration was substantially increased by the P9 treatment of wild-type (WT) mice, but not of IL-6-KO mice (Fig. 4c). Interestingly, the expression of *Icam2* mRNA was lower in IL-6-KO mice (Fig. 4d), which suggests

that normal ICAM-2 expression may require IL-6. An overview for graphical summary is shown in Fig. 4e.

Previous studies have focused on the outer membrane of *A. muciniphila* and have characterized 79 proteins that might represent candidates that mediate an interaction with the host and have metabolic effects⁴⁵. A comparison between the proteins of the outer membrane of *A. muciniphila* and those of our proteomic analysis of the CFS had only one protein in common (Amuc_0576), suggesting that the proteins secreted by *A. muciniphila* differ from those that are present in the outer membrane. The similarity between the nine proteins derived from SNUG-61027 and ATCC-BAA-835 was >98%, and the P9 sequence was 99.41% similar. To identify homologues of P9 or functionally similar peptides in human gut microbiota, we compared the entire human gut metagenome (GenBank:

PPYE01311095.1) with the P9 sequence and found 99.78% query coverage and 100% sequence similarity, indicating that this protein is also present in human gut microbiota.

Receptors involved in GPCR signalling mediate the secretion of GLP-1 from enteroendocrine cells^{46–48}. However, ICAM-2 (also known as CD102) is principally known as an immune cell integrin that is involved in the immune cell interactions that are required for cell barrier penetration⁴⁹. Here, we propose a function of ICAM-2, whereby it acts as a GPCR-like signalling molecule for P9 and mediates the release of GLP-1 from enteroendocrine cells. Although SCFAs are well known as GLP-1 inducers and SCFAs act on GPCR signalling pathway, acetate and propionate produced by *A. muciniphila* could not induce GLP-1 as robustly as P9 in our study. These results indicate that P9 acts on ICAM-2 through a different signal cascade distinctly with SCFAs to induce GLP-1. Furthermore, our findings are consistent with the notion that glucose-induced GLP-1 secretion is mediated by the activation of intracellular Ca²⁺ signalling^{50,51} and CREB- and PLC-mediated pathways^{52–54}. Further studies must determine how ICAM-2 might activate GPCR-like downstream signalling and induce GLP-1 secretion.

IL-6 has multiple tissue-specific effects that are achieved in a paracrine or endocrine manner. Hepatic disruption of IL-6 signalling causes insulin resistance⁵⁵, and BAT-derived IL-6 is required for the effects of BAT transplantation on glucose homeostasis⁵⁶. More recently, it was shown that an acute exercise-induced increase in IL-6 delays gastric emptying, thereby reducing postprandial insulin secretion in humans⁵⁷. In accordance with the findings of previous studies that *A. muciniphila* induces higher IL-6 expression in human-derived peripheral blood mononuclear cells⁴², and that *A. muciniphila*-derived extracellular vesicles induce IL-6 in a dose-dependent manner⁵⁸, here *A. muciniphila* induced the secretion of IL-6 from the gut through P9, which has beneficial effects on metabolic homeostasis. Furthermore, P9 is produced by *A. muciniphila* and its metabolic effects act through IL-6. Moreover, host thermogenesis is prevented when either GLP-1R or IL-6 signalling is inhibited. These results demonstrate that P9 is directly involved in the effects of *A. muciniphila* on IL-6 and GLP-1 signalling.

Despite the positive effects of P9, it should be considered that sustaining P9 in an ecologically competitive harsh condition under an HFD could be challenging if *A. muciniphila* could not outcompete other bacteria in vivo. In humans, GLP-1 is actively degraded within 2 min (ref. ⁵⁹) and, to circumvent this limitation, many studies have focused on developing synthetic GLP-1 agonists that are resistant to degradation by dipeptidyl peptidase 4 inhibitors. GLP-1 receptor agonists are currently recommended as an add-on therapy to metformin for patients with type-2 diabetes and may be used as a monotherapy in patients who cannot tolerate metformin⁶⁰. However, daily subcutaneous injection of a GLP-1 agonist is associated with some adverse effects, including nausea, vomiting, diarrhoea and other gastrointestinal symptoms⁶¹. We found that oral administration of P9 in mice substantially improved glucose homeostasis. The structure of the protein and its safety with regard to its potential therapeutic use are presently under investigation.

Methods

Isolation and cultivation of *A. muciniphila* strains. *A. muciniphila* (ATCC-BAA-835), purchased from the American Type Culture Collection (ATCC), was streaked onto brain–heart infusion (BHI) agar supplemented with 0.5% porcine mucin and 0.05% cysteine in an anaerobic workstation (Coy Laboratory Products). After incubation for 48 h at 37 °C in an anaerobic jar using the GasPack 100 system (BD Bioscience), bacteria were collected from the plates, suspended in anaerobic phosphate-buffered saline (PBS) containing glycerol, and then aliquoted and stored at –80 °C. *A. muciniphila* suspended in 200 µl anaerobic PBS (4.0 × 10⁸ colony-forming units per mouse) was orally administered to mice. *A. muciniphila* (SNUG-61027) was isolated from freshly collected faecal samples that were obtained from three healthy individuals who had not been treated with antibiotics during the preceding year. Each stool sample was mixed

together, cultured in a bioreactor for 2 d and then inoculated into BHI medium supplemented with 5% human serum. After streaking twice more, a single colony was picked. All of the procedures were performed under anaerobic conditions. A list of the characteristics of each volunteer from which *A. muciniphila* was isolated is provided in Supplementary Table 2a. Whole-genome sequencing showed that the mean nucleotide identity between two bacterial colonies was 99.08%, which implies that they were identical. Furthermore, 16S-rRNA sequence Basic Local Alignment Search Tool analysis showed that this isolate was 100% similar to the ATCC-BAA-835.

By direct streaking, *A. muciniphila* (SNUG-61027) was inoculated onto BHI agar (BD Bioscience) supplemented with 0.5% porcine mucin (Sigma-Aldrich) and 0.05% cysteine (Sigma-Aldrich). After incubating for 48 h, a single colony was picked and cultured in BHI broth medium containing 5% FBS for 36 h, and then subcultured in fresh medium. SNUG-61027 grown in FBS-based BHI broth medium was used for supernatant fractionation. To maintain anaerobic conditions, all of the procedures were performed in an anaerobic chamber (Coy Laboratory Products). *Lactobacillus* spp. and *Bifidobacterium* spp. were obtained from KCTC (Korean Collection for Type Culture) or isolated from either healthy fresh infant faeces or frozen adult faeces using BL agar (Kisan Biotech), *Bifidus* Selective Medium (BSM; Sigma-Aldrich) and TOS-propionate agar (Sigma-Aldrich) in an anaerobic chamber. The characteristics of the donors from whom faecal samples were provided are shown in Supplementary Table 2b. Bacteria were cultured in MRS broth for 24 h and then subcultured for another 24 h before being used in cell culture experiments.

Experimental animals. C57BL/6J mice (SLC) were housed (no more than four per cage) in a pathogen-free animal facility under a 12 h–12 h light–dark cycle and were given free access to food and water. Male mice (aged 6 weeks) were fed either a low-fat diet (D12450K, Research Diets) or a HFD (D12492, Research Diets), or were fed an HFD and were also administered daily with *A. muciniphila* for 14 weeks. At the end of the treatment period, the mice were euthanized and analysed. The group sizes were $n = 7–10$ mice per condition, based on a previous study⁷. The mice were matched for body mass and randomized to groups before each experiment and the variance in each dataset was compared between the groups using Barlett's test. Experiments were not performed in a blinded manner. Food intake and body mass were measured once each week.

The purified protein from *A. muciniphila*, P9 (100 µg per mouse) was orally (or intraperitoneally) administered to a second cohort of mice during HFD feeding and the results were compared with those of the HFD-fed group. The mice were euthanized at 8 weeks and then analysed ($n = 8$ (low-fat diet), $n = 8$ (HFD), $n = 8$ (HFD + P9)). The effects of P9 were also analysed in IL-6-KO HFD-fed mice, and the results were compared with those of WT mice that were administered P9. IL-6-KO mice (Jackson Laboratory) from the C57BL/6J background were used and age-matched (6 weeks) and sex-matched (male) WT mice of the same background were used as controls (WT: $n = 8$ (HFD), $n = 8$ (HFD + P9); IL-6-KO: $n = 6$ (HFD), $n = 6$ (HFD + P9)). All of the mice were initially acclimated to their environment for 1 week while consuming a normal chow diet and were raised in the same facility under the same conditions. The effects of the HFD on the metabolism—including blood glucose, weight gain and food intake—were similar in the IL-6-KO and WT mice (Extended Data Fig. 10a,b). At the end of the experiments, the animals were anaesthetized with isoflurane and blood samples were collected by retro-orbital sinus puncture, then the mice were killed by cervical dislocation.

Glucose and insulin tolerance testing. Glucose tolerance testing was performed using oral gavage of 2 g kg⁻¹ body mass or i.p. administration of 1 g kg⁻¹ body mass glucose after 16 h of fasting (2200–1400). Blood samples were collected by tail-tip bleeding 0, 15, 30, 60, 90 and 120 min later, and the blood glucose concentrations were measured using a glucometer (Accu-Check Performa; Roche Diagnostics). Intraperitoneal insulin tolerance testing was performed 1 week after the intraperitoneal glucose tolerance testing. Mice were fasted for 5 h (0900–1400), insulin (Humulin R, Eli Lilly) was next injected at a concentration of 0.5 U kg⁻¹ body mass, and then their blood glucose concentrations were measured, as described above.

Serum insulin measurements. To measure serum insulin concentration, blood samples were allowed to clot for 30 min at room temperature, then serum was separated by centrifugation at 4,000g for 10 min and stored at –80 °C. Serum insulin concentration was measured using the Ultra-Sensitive Mouse Insulin ELISA kit (Crystal Chem).

Plasma GLP-1 measurements. For the measurement of plasma GLP-1, mice were fasted for 5 h in the morning. Blood samples were obtained by retro-orbital sinus puncture 0 min and 10 min after oral gavage of 2 g kg⁻¹ body mass glucose and collected into prechilled EDTA-coated tubes containing 1 µg ml⁻¹ diprotin A (6019; Tocris Bioscience), centrifuged without delay, and the plasma was then separated and stored at –80 °C. To measure GLP-1 after a single administration, male mice (aged 8 weeks) were fasted for 5 h in the morning. A single dose of each respective group (PBS, P9, EcPrc, sodium acetate (S2889; Sigma-Aldrich) and sodium propionate (P1880; Sigma-Aldrich)) was administered i.p. at 300 µg

per mouse and blood samples were obtained by cardiac puncture 10 min after oral gavage of 2 g kg⁻¹ body mass glucose. The collected blood was collected into prechilled EDTA-coated tubes containing 1 µg ml⁻¹ diprotin A (Tocris Bioscience) and 500 Kallikrein inhibitor units of aprotinin (A6279; Sigma-Aldrich) and plasma was separated by centrifugation at 4,000g for 10 min then stored at -80 °C. GLP-1 concentration was determined using the GLP-1 ELISA kit (RayBiotech).

RNA isolation and RT-qPCR analysis. RNA was extracted from tissues using the Easy-spin Total RNA extraction kit (iNTRON Biotechnology). RNA was reverse-transcribed using the LeGene cDNA synthesis master mix (LeGene) according to the manufacturer's instructions. The relative mRNA expression levels were determined by qPCR using the Rotor-Gene Q (Qiagen) or QuantStudio 6 flex Real-Time PCR system (Thermo Fisher Scientific). A list of the sequences of the primers used for RT-qPCR is provided in Supplementary Table 4.

Histological analysis. The epididymal, interscapular and inguinal fat pads were fixed in 4% formaldehyde, processed into paraffin blocks, sectioned and stained with H&E. The slides were scanned under a light microscope using Imaging Sys (Nikon). The mean adipocyte size was measured using Image Scope (LEICA Biosystems).

Temperature measurements. The skin temperature over the iBAT was recorded using an infrared camera (T420 Compact Infrared Thermal Imaging Camera; FLIR) and analysed using the FLIR tools software. Eight mice per group were briefly anaesthetized using isoflurane, and the mean temperature of the area surrounding the iBAT was recorded from each picture and analysed. Rectal temperature was measured using a digital thermometer (Testo 925, Testo) according to the manufacturer's protocol. To cold-stress the mice, they were individually placed in a humidity-controlled chamber at 5 °C and 40–60% humidity.

Flow cytometric analysis. To isolate adipocytes from the iBAT of each mouse ($n = 8$ per group), the interscapular adipose tissue was dissected, minced finely with scissors and digested in Hank's balanced salt solution (HBSS) containing collagenase (1 mg ml⁻¹ collagenase type II, 0.5% bovine serum albumin (BSA)) at 37 °C for 30 min. The cells were then passed through a cell strainer (100 µm), washed twice with PBS and the red blood cells were lysed. The cells were next washed with cold PBS and incubated with staining cocktail (CD45-APC-Cy7 (BD557659), 7AAD-PerCP-Cy5.5 (BD559925), CD11b-PE-Cy7 (BD561098) and CD206-Alexa Fluor 647 (BD565250) (BD Bioscience)) diluted at 1:200 in FACS buffer (2% FBS in PBS) for 20 min on ice in the dark. The cells were then washed and analysed using the FACS Verse flow cytometer (BD Bioscience) and the data were analysed using FlowJo v.10.4.2. The gating strategy for detecting M2-like macrophages (CD11b⁺CD206⁺) in the iBAT is described in Extended Data Fig. 2i.

Cell culture and measurement of GLP-1 secretion. The NCI-H716 human intestinal cell line was obtained from the ATCC (ATCC-CCL-251) and cultured in RPMI 1640 supplemented with 10% FBS (GenDEPOT) and 1% penicillin-streptomycin (Life Technologies) at 37 °C under 5% CO₂. The GLUTag cell line was a gift from D. J. Drucker, University of Toronto, and was cultured in Dulbecco's modified Eagle's medium (DMEM) containing 10% FBS and 1% penicillin-streptomycin at 37 °C under 5% CO₂. For the GLP-1-secretion assay, the cells were cultured in collagen-coated 96-well plates (3 × 10⁵ cells per ml) overnight. On the day of treatment, the cells were starved in HBSS containing 0.2% BSA for 2 h, and then treated with bacterial pellets or supernatants for 2 h. The cell supernatants were then collected for the measurement of GLP-1 concentration. The RAW 264.7 and CT26 cell lines were purchased from the Korean Cell Line Bank and cultured in DMEM containing 10% FBS and 1% penicillin-streptomycin. Immortalized BACs were provided by Kai Ge⁶² (NIDDK, National Institutes of Health (NIH)) and maintained in DMEM containing 10% FBS and 1% penicillin-streptomycin. Each cell line was authenticated by morphology and growth characteristics as well as manufacturing companies, and was assessed for mycoplasma contamination regularly. *E. coli* lipopolysaccharide (L2630) was obtained from Sigma-Aldrich.

Human intestinal epithelial cell culture and treatment. Primary human intestinal epithelial cells (CC-2931, frozen vial of 800,000 cells) were purchased from Lonza and authenticated by Lonza. Cells were grown using the SmGM-2 BulletKit (CC-3182) with supplements (CC-4149) provided by Lonza. Cells were seeded into a 96-well flat-bottomed collagen-coated plate at 5 × 10⁴ cells per well and incubated overnight. On the day of treatment, the cells were starved in HBSS containing 0.2% BSA for 1 h and then treated with P9 (50 µg ml⁻¹) for 1 h. The cell supernatants were then collected for the measurement of GLP-1 concentration and the cell pellets were obtained for qPCR analysis.

Isolation of primary mouse preadipocytes. To isolate primary BACs, interscapular adipose tissue was dissected from male C57BL/6j mice. Six depots were pooled, minced finely with scissors and digested for 30 min in HBSS containing collagenase (1 mg ml⁻¹ collagenase type II, 2% BSA, 25 mM HEPES) at 37 °C for 30 min. To stop the enzymatic activity, 10% FBS-containing medium was

added and the mixture was passed through a cell strainer (100 µm). The cells were then washed twice with PBS, and the red blood cells were lysed. The cells obtained were seeded into 12-well plates with prewarmed DMEM containing 4.5 g l⁻¹ glucose (HyClone Laboratories), 20% FBS (GenDEPOT) and 1% penicillin-streptomycin. Floating cells were removed the next day, fresh prewarmed culture medium was added, and the samples were prepared for FACS analysis or qPCR analysis was performed after IL-6 treatment.

Bacterial supernatant filtrate preparation. The supernatant was collected from a 150 ml culture of *A. muciniphila* (SNUG-61027) and filtered using filters with a number of differing pore sizes and molecular-mass cut-offs. Swing-bucket centrifugation (Eppendorf 5415R centrifuge; Eppendorf) was used for all of the procedures. The supernatants were centrifuged at 7,000g for 10 min at 4 °C and then passed through polyethersulfone filters (0.22 µm; Merck Millipore) to remove the residual bacterial cells. The derived filtrates were then passed through 1,000 kDa filters (Vivaspin 20 polyethersulfone ultrafiltration unit; Sartorius) at 6,000g for 30 s. The 1,000 kDa filtrates were then loaded onto 300 kDa filters (Sartorius) and centrifuged at 6,000g for a further 30 s. The 300 kDa filtrates were then passed through 100 kDa, 30 kDa and 10 kDa filters (Pall Microsep Centrifugal Device; Pall) at 3,200g for 10 min. Each filtrate (500 µl) was frozen at -80 °C until assayed.

The BCA Protein Assay kit (Thermo Fisher Scientific) was used to determine the protein content of each filtrate, according to the manufacturer's instructions. Proteinase K (iNTRON Biotechnology) was also added to a portion of the 100 kDa filtrate at 100 µg ml⁻¹, which was incubated at 55 °C for 1 h, and then the enzyme activity was inactivated at 90 °C for 10 min.

FPLC analysis. To further separate the proteins of interest in the fractions from bulk proteins, chromatography was performed using an AKTA Explorer fast protein LC (FPLC) system (GE Healthcare Bio-Sciences). The FPLC system was equipped with a sample loop of 2.0 ml and a Mono Q anion-exchange column of 5 × 50 mm (GE Healthcare), with a column volume of 1 ml column volume. Buffer A (10 mM potassium phosphate and 50 mM NaCl) and buffer B (10 mM potassium phosphate and 1 M NaCl) were prepared. The 100 kDa filtrate and control medium, each containing 25 mg protein, were applied to the FPLC system at a flow rate of 1 ml per min, with continuous monitoring of the absorbance at 280 nm. Twenty-six fractions were collected. After identifying the functional fractions using a GLP-1-secretion assay, they were selected and concentrated using a 30 kDa Microsep centrifugal device (Pall). For size-exclusion chromatography (gel permeation chromatography (GPC)/SEC), the AKTA Explorer FPLC system was equipped with a GPC column with a column volume of 120 ml. Buffer A (10 mM potassium phosphate and 50 mM NaCl) was prepared. The samples were loaded at 3 ml min⁻¹ with continuous monitoring, and 40 fractions were collected and stored at -80 °C until analysis.

LC-MS/MS analysis. The fractions of the *A. muciniphila* culture supernatant were sent to the Proteomics Core Facility at Seoul National University Hospital in Seoul, Korea for protein identification and analysis. The samples were analysed using an LC-MS instrument consisting of an Ultimate 3000 RSLC system (Dionex), coupled via a nano-electrospray ion source (Thermo Fisher Scientific) to a Q Exactive plus Orbitrap (Thermo Fisher Scientific), according to previously described procedures⁶³. MS raw files were searched using Maxquant software (v.1.6.1.0)⁶⁴ and the Andromeda search engine⁶⁵ against the UniProt reference proteome database (*A. muciniphila*; UP000001031) and the UniProt reference proteome database (*Bos Taurus*; UP000009136). The false-discovery rate was set to 0.01 for both proteins and peptides with a minimum length of six amino acids, and was determined by searching a reverse database.

Plasmid constructs and protein expression. The nucleotide sequences of the following genes were obtained by whole-genome sequencing (Supplementary Table 5) conducted at Macrogen using the isolated *A. muciniphila* strain SNUG-61027: *pgk* (UniProt: B2UKW8), *Amuc_0017* (UniProt: B2UL75), *fucl* (UniProt: B2UN39), *Amuc_0405* (UniProt: B2UND1), *Amuc_1282* (UniProt: B2URM2), *glsA* (UniProt: B2UL96), *Amuc_1829* (UniProt: B2UN36), *Amuc_0576* (UniProt: B2UPD6) and *Amuc_1631* (UniProt: B2UM07). The homologous protein to P9 was identified in *E. coli* DH5α (*EcPrc*) in the UniProt database (<https://www.uniprot.org/>). The *Amuc_1100*-expressing plasmid was previously described⁷. Each of the corresponding cDNAs was cloned into the pET-26b plasmid (Novagen), which contains an isopropyl β-D-1-thiogalactopyranoside (IPTG)-inducible promoter. A list of the primer sequences used to generate the construct is provided in Supplementary Table 6. Sequences in bold are restriction sites for the NdeI and XhoI enzymes (Thermo Fisher Scientific). A His-tag was added to the C terminus of each protein for subsequent purification. The correct sequences of the resulting plasmids were then confirmed. These vectors were transfected into BL21 *Escherichia coli* (RRID: WBHT115(DE3)) and grown in LB broth containing kanamycin (50 µg ml⁻¹), into which 1.0 mM IPTG was added during the mid-exponential growth stage, after which a further 4 h was provided for protein expression. The cells were pelleted by centrifuging for 10 min at 10,733g and the cell pellets were stored at -80 °C until lysis. The cell pellets were resuspended

and lysed by sonication (Vibracell VCX500, Sonics & Materials). For protein purification, TALON Metal Affinity resin and the HisTALON buffer kit (Takara Bio USA) were used according to the manufacturer's instructions, with minor modifications. The purified proteins were then dialysed against endotoxin-free distilled water. Removal of endotoxin from the purified protein solution was accomplished by treatment with 1% Triton X-114 (Sigma-Aldrich) for 30 min at 4°C. The phase containing the endotoxin was separated by centrifugation at 12,000 r.p.m. for 10 min. This procedure was repeated three times. The purified proteins were then incubated three times with SM-2 beads (Bio-Rad Laboratories) for 1 h at 4°C to remove residual Triton X-114. The purification of each protein was confirmed using SDS-polyacrylamide gel electrophoresis and Coomassie blue staining by the presence of single band of the expected size.

RNA-seq analysis. RNA was extracted from NCI-H716 cells after treatment with P9 (50 µg ml⁻¹) for 30 min and then processed for RNA-seq analysis at Macrogen. Macrogen's application, which is based on the Illumina sequencing protocol, was used to analyse the transcriptome. Three control and three treatment samples were analysed. Differentially expressed genes were defined as showing >1.5-fold changes in expression, with $P < 0.05$. The use of these criteria resulted in the selection of 25 differentially expressed genes. Gene set enrichment analysis was performed using Gene Ontology and the KEGG database. Of the 27,685 genes identified, 12,019 with at least one zero fragments per kilobase of transcript per million mapped reads were excluded, which left 15,666 genes to be processed for Gene Ontology analysis.

Calcium measurement. A Fluo-4 NW Assay kit (Thermo Fisher Scientific) was used to measure intracellular calcium influx on a Flexstation 3 microplate reader (Molecular Devices). Cells were seeded onto poly-L-lysine-coated (Sigma-Aldrich) 96-well black-walled plates at 2×10^4 cells per well and incubated overnight. The next day, the growth medium was replaced with 100 µl probenecid per well to prevent the extrusion of the dye from the cells, and the cells were then incubated for 30 min at 37°C and at room temperature for a further 30 min. Flexstation 3 was used to analyse the calcium influx (excitation/emission, 485 nm/535 nm).

LRC analysis based on TriCEPS. TriCEPS (Dualsystems Biotech) was used for LRC analysis, as previously described⁶⁶. TriCEPS was left to bind to the ligand in pH 8.2, 25 mM HEPES solution at room temperature with gentle shaking for 90 min, and then this was added to oxidized NCI-H716 cells, which were incubated at 4°C in the dark for 90 min on a rotator. After centrifugation, the cell pellets were collected and, under ice-cold conditions, were sent for LC-MS/MS analysis at Dualsystems Biotech. LRC data were analysed using a statistical ANOVA model⁶⁷ and the adjusted P value for the differential abundance of each protein was plotted against the magnitude of the fold-enrichment.

Antibody inhibition test. GLUTag and NCI-H716 cells were incubated with an ICAM-2-blocking peptide (MBS823225; MyBioSource), anti-ICAM-2 antibodies (BD Pharmingen, 3C4 (mIC2/4); BD553326), anti-total KTN1 antibodies (A44072; Antibody Solutions) or a negative control antibody (mouse anti-β tubulin (32-2600); Thermo Fisher Scientific) for 1 h, before P9 (50 µg ml⁻¹) treatment for 1 h, and the supernatants were then collected and stored at -80°C until they were assayed.

Caecal metabolite analysis. For nuclear magnetic resonance (NMR)-based metabolomic analysis, caecal contents (50–100 mg) were mixed with 600 µl deionized distilled water, vortexed and homogenized using a tissue homogenizer. After centrifugation (14,000g at 4°C) for 10 min, 60 µl of deuterium oxide (containing 0.025 mg ml⁻¹ 3-(trimethylsilyl) propionic acid-*d*4 sodium salt, 60 µl of 1 mM imidazole, 60 µl of 2 mM Na₃N₃ and 120 µl of 0.5 M KH₂PO₄) were added to 300 µl of the supernatant. The mixtures were vortexed for 1 min and centrifuged at 14,000g for 10 min. The clear supernatants were then transferred to NMR tubes (5 mm; Wilmad-Lab Glass) for NMR analysis. The ¹H-NMR spectra were acquired using a Varian 500 MHz NMR system (Varian) spectrometer equipped with a cold flow-probe. ¹H-NMR spectra were collected at 25°C using the water presaturation pulse sequence. Spectra were collected with 64 transients using a 4 s acquisition time and a 2 s recycle delay. Tentative assignments of ¹H NMR signals were performed using Chenomx NMR Suite v.8.3 (Chenomx), according to the Human Metabolome Database and a previous publication⁶⁸.

Analysis of and bioinformatics pipeline for the caecal microbiota. The caecum of each mouse was collected in a sterile tube, immediately frozen in liquid nitrogen and stored at -80°C until further use. DNA was extracted using the QiaAmp Fast DNA Stool Mini Kit (Qiagen), with slight modification of the manufacturer's protocol. Caecal samples were also homogenized with stainless steel beads (5 mm; Qiagen) after homogenization with glass beads (0.1 mm). Illumina-adapted universal primers 515F/806R, which target the V4 region of the 16S rRNA, were used for DNA amplification, and the DNA was then purified using the QIAquick PCR purification Kit (Qiagen). Purified amplicons were quantified using the KAPA Library Quantification Kit (KAPA Biosystems). The concentration of each sample was normalized to 4 nM, and they were then pooled into a single tube

and sequenced on the MiSeq platform using a paired-end 2 × 300 bp reagent kit (Illumina). Raw reads were demultiplexed using CASAVA (v.1.8) and imported into the QIIME2 pipeline (v.2020.2). Low-quality sequences, duplicated sequences and chimeric sequences were eliminated using Divisive Amplicon Denoising Algorithm 2 (DADA2). Sequences were classified into operational taxonomic units at the 99% similarity level against the Greengenes 13.8 database using the closed-reference method. The ALDEx2 package in R was used to compare the differential abundance of taxonomic units in the HFD and HFD + *A. muciniphila* groups.

Indirect calorimetry and body composition measurements. C57BL/6J mice were fed a 60% HFD and were orally administered 200 µl of P9 (100 µg per mouse) or the same volume of endotoxin-free distilled water for 10 d. The mice were individually placed into metabolic chambers (Oxylet system, Panlab-Harvard Apparatus) and acclimated for 2 d before measurements were made. Oxygen consumption (VO₂) and carbon dioxide production (VCO₂) were calculated every 3 min using METABOLISM (v.2.2.01, Panlab-Harvard Apparatus). The respiratory quotient (RQ) was calculated as VCO₂/VO₂ and energy expenditure (EE) was calculated using the following formula: EE = VO₂ × 1.44 × (3.815 + 1.232 × RQ). Fatty acid oxidation was calculated using the following formula: (1.6946 × VO₂) - (1.7012 × VCO₂). The body composition of the animals (percentage of fat mass and lean mass) was also measured after the indirect calorimetry measurements using the Minispec LF90 Analyzer (Bruker Optics), according to the manufacturer's instructions. Body mass was measured before these measurements to enable the calculation of the fat and lean-mass percentages.

GLP-1R β-arrestin assay. For the β-arrestin assay, HTLA cells (HEK293 cell line stably expressing a tTA-dependent luciferase reporter and a β-arrestin2-TEV fusion gene)⁶⁹ were a gift from B. L. Roth and were maintained in DMEM with 10% FBS, penicillin (100 U ml⁻¹), streptomycin (100 µg ml⁻¹), puromycin (2 µg ml⁻¹) and hygromycin B (100 µg ml⁻¹) in a humidified atmosphere at 37°C in 5% CO₂. The confluent HTLA cells were transfected with 5 µg of GLP-1R-Tango and 500 ng of pRL-SV40P construct (66295, 27163; Addgene) using Lipofectamine 3000 (L3000015; Invitrogen). The next day, transfected cells were transfected at 40,000 cells per well into poly-L-lysine-coated 96-well plates. After overnight incubation, exendin-4 (1933; Tocris Bioscience) or P9 was prepared and diluted in HBSS with 20 mM HEPES (pH 7.4), then exendin-4 (50 µM) or P9 (50 µg ml⁻¹) was administered to HTLA cells for 24 h. Next, the cells were washed, lysed and analysed by luminescence using the Infinite 200 Pro microplate reader (Tecan Group) and the Dual-Glo Luciferase Assay System (2920; Promega). The luciferase activities were normalized to *Renilla* luminescence and relative activity were calculated.

Ethics statement. The experimental procedures were reviewed and approved by the Institutional Animal Care and Use Committee of Seoul National University (SNU-180723-1-1). All of the experiments were performed in accordance with the relevant guidelines and regulations and were approved by the Institutional Review Board of Seoul National University (IRB No 1405/002-008) and Samsung Medical Center (SMC 2014-11-023-001).

Statistical analysis. All data are expressed as the mean ± s.e.m. Mouse groups were compared using one-way or two-way ANOVA, followed by Tukey's post hoc test or the unpaired t -test. For in vitro data, the Kruskal-Wallis, followed by Dunn's post hoc test or the Mann-Whitney U -test was performed. Statistical analysis was performed using GraphPad Prism v.7.04. Statistical significance is indicated by asterisks (*) or phi (°); ° or * $P < 0.05$, °° or ** $P < 0.01$, °°° or *** $P < 0.001$, °°°° or **** $P < 0.0001$.

Reporting Summary. Further information on research design is available in the Nature Research Reporting Summary linked to this article.

Data availability

RNA-seq data and 16S rRNA gene sequencing data that support the findings of this study have been deposited at the European Nucleotide Archive (ENA) and are publicly available under the accession numbers PRJEB36198 (RNA-seq) and PRJEB36225 (16S rRNA gene sequencing). Whole-genome sequencing data of SNUG-61027 is deposited at the ENA under accession number PRJEB42664 and is publicly available. Similarly, metabolomic data were deposited at MetaboLights under accession number MTBLS1824 and are publicly available. Source data are provided with this paper.

Received: 16 March 2020; Accepted: 16 February 2021;

Published online: 05 April 2021

References

- Geach, T. Gut microbiota: mucin-munching bacteria modulate glucose metabolism. *Nat. Rev. Endocrinol.* **13**, 66 (2017).
- Chevalier, C. et al. Gut microbiota orchestrates energy homeostasis during cold. *Cell* **163**, 1360–1374 (2015).

3. Parekh, P. J., Balart, L. A. & Johnson, D. A. The influence of the gut microbiome on obesity, metabolic syndrome and gastrointestinal disease. *Clin. Transl. Gastroenterol.* **6**, e91 (2015).
4. Sonnenburg, J. L. & Backhed, F. Diet–microbiota interactions as moderators of human metabolism. *Nature* **535**, 56–64 (2016).
5. Everard, A. et al. Cross-talk between *Akkermansia muciniphila* and intestinal epithelium controls diet-induced obesity. *Proc. Natl Acad. Sci. USA* **110**, 9066–9071 (2013).
6. Cani, P. D. et al. Endocannabinoids—at the crossroads between the gut microbiota and host metabolism. *Nat. Rev. Endocrinol.* **12**, 133–143 (2016).
7. Plovier, H. et al. A purified membrane protein from *Akkermansia muciniphila* or the pasteurized bacterium improves metabolism in obese and diabetic mice. *Nat. Med.* **23**, 107–113 (2017).
8. Depommier, C. et al. Supplementation with *Akkermansia muciniphila* in overweight and obese human volunteers: a proof-of-concept exploratory study. *Nat. Med.* **25**, 1096–1103 (2019).
9. The GBD 2015 Obesity Collaborators. Health effects of overweight and obesity in 195 countries over 25 years. *N. Engl. J. Med.* **377**, 13–27 (2017).
10. Lim, M. Y. et al. The effect of heritability and host genetics on the gut microbiota and metabolic syndrome. *Gut* **66**, 1031–1038 (2017).
11. Dao, M. C. et al. *Akkermansia muciniphila* and improved metabolic health during a dietary intervention in obesity: relationship with gut microbiome richness and ecology. *Gut* **65**, 426–436 (2016).
12. Karlsson, C. L. et al. The microbiota of the gut in preschool children with normal and excessive body weight. *Obesity* **20**, 2257–2261 (2012).
13. Santacruz, A. et al. Gut microbiota composition is associated with body weight, weight gain and biochemical parameters in pregnant women. *Br. J. Nutr.* **104**, 83–92 (2010).
14. Dao, M. C. et al. *Akkermansia muciniphila* abundance is lower in severe obesity, but its increased level after bariatric surgery is not associated with metabolic health improvement. *Am. J. Physiol. Endocrinol. Metab.* **317**, E446–E459 (2019).
15. Zhang, L. et al. *Akkermansia muciniphila* can reduce the damage of gluco/lipotoxicity, oxidative stress and inflammation, and normalize intestine microbiota in streptozotocin-induced diabetic rats. *Pathog. Dis.* <https://doi.org/10.1093/femspd/fty028> (2018).
16. Liu, J. et al. Gypenosides reduced the risk of overweight and insulin resistance in C57BL/6J mice through modulating adipose thermogenesis and gut microbiota. *J. Agric. Food Chem.* **65**, 9237–9246 (2017).
17. Gao, X. et al. Polyphenol- and caffeine-rich postfermented pu-erh tea improves diet-induced metabolic syndrome by remodeling intestinal homeostasis in mice. *Infect. Immun.* <https://doi.org/10.1128/IAI.00601-17> (2018).
18. Depommier, C. et al. Pasteurized *Akkermansia muciniphila* increases whole-body energy expenditure and fecal energy excretion in diet-induced obese mice. *Gut Microbes* <https://doi.org/10.1080/19490976.2020.1737307> (2020).
19. Gribble, F. M. & Reimann, F. Function and mechanisms of enteroendocrine cells and gut hormones in metabolism. *Nat. Rev. Endocrinol.* **15**, 226–237 (2019).
20. Greiner, T. U. & Backhed, F. Microbial regulation of GLP-1 and L-cell biology. *Mol. Metab.* **5**, 753–758 (2016).
21. Wang, L. et al. A purified membrane protein from *Akkermansia muciniphila* or the pasteurised bacterium blunts colitis associated tumourigenesis by modulation of CD8⁺ T cells in mice. *Gut* <https://doi.org/10.1136/gutjnl-2019-320105> (2020).
22. Tolhurst, G. et al. Short-chain fatty acids stimulate glucagon-like peptide-1 secretion via the G-protein-coupled receptor FFAR2. *Diabetes* **61**, 364–371 (2012).
23. Psichas, A. et al. The short chain fatty acid propionate stimulates GLP-1 and PYY secretion via free fatty acid receptor 2 in rodents. *Int. J. Obes.* **39**, 424–429 (2015).
24. Li, Z. et al. Butyrate reduces appetite and activates brown adipose tissue via the gut-brain neural circuit. *Gut* **67**, 1269–1279 (2018).
25. Yadav, H., Lee, J. H., Lloyd, J., Walter, P. & Rane, S. G. Beneficial metabolic effects of a probiotic via butyrate-induced GLP-1 hormone secretion. *J. Biol. Chem.* **288**, 25088–25097 (2013).
26. Chambers, E. S. et al. Effects of targeted delivery of propionate to the human colon on appetite regulation, body weight maintenance and adiposity in overweight adults. *Gut* **64**, 1744–1754 (2015).
27. Lund, M. L. et al. L-cell differentiation is induced by bile acids through GPBAR1 and Paracrine GLP-1 and serotonin signaling. *Diabetes* **69**, 614–623 (2020).
28. Albaugh, V. L. et al. Role of bile acids and GLP-1 in mediating the metabolic improvements of bariatric surgery. *Gastroenterology* **156**, 1041–1051 (2019).
29. Brighton, C. A. et al. Bile acids trigger GLP-1 release predominantly by accessing basolaterally located G protein-coupled bile acid receptors. *Endocrinology* **156**, 3961–3970 (2015).
30. Chimerel, C. et al. Bacterial metabolite indole modulates incretin secretion from intestinal enteroendocrine L cells. *Cell Rep.* **9**, 1202–1208 (2014).
31. Lebrun, L. J. et al. Enteroendocrine L cells sense LPS after gut barrier injury to enhance GLP-1 secretion. *Cell Rep.* **21**, 1160–1168 (2017).
32. Gribble, F. M. & Reimann, F. Enteroendocrine cells: chemosensors in the intestinal epithelium. *Annu. Rev. Physiol.* **78**, 277–299 (2016).
33. Ténenbaum, N. et al. Bacterial ClpB heat-shock protein, an antigen-mimetic of the anorexigenic peptide α -MSH, at the origin of eating disorders. *Transl. Psychiatry* **4**, e458 (2014).
34. Everard, A. et al. Responses of gut microbiota and glucose and lipid metabolism to prebiotics in genetic obese and diet-induced leptin-resistant mice. *Diabetes* **60**, 2775–2786 (2011).
35. Rooks, M. G. & Garrett, W. S. Gut microbiota, metabolites and host immunity. *Nat. Rev. Immunol.* **16**, 341–352 (2016).
36. Donaldson, G. P. et al. Gut microbiota utilize immunoglobulin A for mucosal colonization. *Science* **360**, 795–800 (2018).
37. Ansaldo, E. et al. *Akkermansia muciniphila* induces intestinal adaptive immune responses during homeostasis. *Science* **364**, 1179–1184 (2019).
38. Shin, N. R. et al. An increase in the *Akkermansia* spp. population induced by metformin treatment improves glucose homeostasis in diet-induced obese mice. *Gut* **63**, 727–735 (2014).
39. Krieger, J. P. et al. Glucagon-like peptide-1 regulates brown adipose tissue thermogenesis via the gut–brain axis in rats. *Am. J. Physiol. Regul. Integr. Comp. Physiol.* **315**, R708–R720 (2018).
40. Beiroa, D. et al. GLP-1 agonism stimulates brown adipose tissue thermogenesis and browning through hypothalamic AMPK. *Diabetes* **63**, 3346–3358 (2014).
41. Lynch, L. et al. iNKT cells induce FGF21 for thermogenesis and are required for maximal weight loss in GLP1 therapy. *Cell Metab.* **24**, 510–519 (2016).
42. Ottman, N. et al. Pili-like proteins of *Akkermansia muciniphila* modulate host immune responses and gut barrier function. *PLoS ONE* **12**, e0173004 (2017).
43. Ellingsgaard, H. et al. Interleukin-6 enhances insulin secretion by increasing glucagon-like peptide-1 secretion from L cells and alpha cells. *Nat. Med.* **17**, 1481–1489 (2011).
44. Kahles, F. et al. GLP-1 secretion is increased by inflammatory stimuli in an IL-6-dependent manner, leading to hyperinsulinemia and blood glucose lowering. *Diabetes* **63**, 3221–3229 (2014).
45. Ottman, N. et al. Characterization of outer membrane proteome of *Akkermansia muciniphila* reveals sets of novel proteins exposed to the human intestine. *Front. Microbiol.* **7**, 1157 (2016).
46. Hauge, M. et al. Gq and Gs signaling acting in synergy to control GLP-1 secretion. *Mol. Cell. Endocrinol.* **449**, 64–73 (2017).
47. Ulven, T. Short-chain free fatty acid receptors FFA2/GPR43 and FFA3/GPR41 as new potential therapeutic targets. *Front. Endocrinol.* **3**, 111 (2012).
48. Husted, A. S., Trauelsen, M., Rudenko, O., Hjorth, S. A. & Schwartz, T. W. GPCR-mediated signaling of metabolites. *Cell Metab.* **25**, 777–796 (2017).
49. Gorina, R., Lyck, R., Vestweber, D. & Engelhardt, B. β 2 integrin-mediated crawling on endothelial ICAM-1 and ICAM-2 is a prerequisite for transcellular neutrophil diapedesis across the inflamed blood–brain barrier. *J. Immunol.* **192**, 324–337 (2014).
50. Kuhre, R. E., Frost, C. R., Svendsen, B. & Holst, J. J. Molecular mechanisms of glucose-stimulated GLP-1 secretion from perfused rat small intestine. *Diabetes* **64**, 370–382 (2015).
51. Flamez, D. et al. Altered cAMP and Ca²⁺ signaling in mouse pancreatic islets with glucagon-like peptide-1 receptor null phenotype. *Diabetes* **48**, 1979–1986 (1999).
52. Lee, J. H., Wen, X., Cho, H. & Koo, S. H. CREB/CRTC2 controls GLP-1-dependent regulation of glucose homeostasis. *FASEB J.* **32**, 1566–1578 (2018).
53. Shin, S. et al. CREB mediates the insulinotropic and anti-apoptotic effects of GLP-1 signaling in adult mouse β -cells. *Mol. Metab.* **3**, 803–812 (2014).
54. Bala, V. et al. Release of GLP-1 and PYY in response to the activation of G protein-coupled bile acid receptor TGR5 is mediated by Epac/PLC-epsilon pathway and modulated by endogenous H2S. *Front. Physiol.* **5**, 420 (2014).
55. Wunderlich, F. T. et al. Interleukin-6 signaling in liver-parenchymal cells suppresses hepatic inflammation and improves systemic insulin action. *Cell Metab.* **12**, 237–249 (2010).
56. Stanford, K. I. et al. Brown adipose tissue regulates glucose homeostasis and insulin sensitivity. *J. Clin. Invest.* **123**, 215–223 (2013).
57. Lang Lehrsrov, L. et al. Interleukin-6 delays gastric emptying in humans with direct effects on glycemic control. *Cell Metab.* <https://doi.org/10.1016/j.cmet.2018.04.008> (2018).
58. Kang, C. S. et al. Extracellular vesicles derived from gut microbiota, especially *Akkermansia muciniphila*, protect the progression of dextran sulfate sodium-induced colitis. *PLoS ONE* **8**, e76520 (2013).
59. Gupta, V. Glucagon-like peptide-1 analogues: an overview. *Indian J. Endocrinol. Metab.* **17**, 413–421 (2013).
60. John B. Buse, J. B. et al. 2019 update to: management of hyperglycemia in type 2 diabetes, 2018. A consensus report by the American Diabetes Association (ADA) and the European Association for the Study of Diabetes (EASD). *Diabetes Care* **43**, 487–493 (2020).

61. Filippatos, T. D., Panagioutopoulou, T. V. & Elisaf, M. S. Adverse effects of GLP-1 receptor agonists. *Rev. Diabet. Stud.* **11**, 202–230 (2014).
62. Park, Y. K. et al. Distinct roles of transcription factors KLF4, Krox20, and peroxisome proliferator-activated receptor γ in adipogenesis. *Mol. Cell. Biol.* <https://doi.org/10.1128/MCB.00554-16> (2017).
63. Lee, H. et al. Quantitative proteomic analysis identifies AHNAK (neuroblast differentiation-associated protein AHNAK) as a novel candidate biomarker for bladder urothelial carcinoma diagnosis by liquid-based cytology. *Mol. Cell. Proteomics* **17**, 1788–1802 (2018).
64. Tyanova, S., Temu, T. & Cox, J. The MaxQuant computational platform for mass spectrometry-based shotgun proteomics. *Nat. Protoc.* **11**, 2301–2319 (2016).
65. Cox, J. et al. Andromeda: a peptide search engine integrated into the MaxQuant environment. *J. Proteome Res.* **10**, 1794–1805 (2011).
66. Frei, A. P. et al. Direct identification of ligand-receptor interactions on living cells and tissues. *Nat. Biotechnol.* **30**, 997–1001 (2012).
67. Frei, A. P., Moest, H., Novy, K. & Wollscheid, B. Ligand-based receptor identification on living cells and tissues using TRICEPS. *Nat. Protoc.* **8**, 1321–1336 (2013).
68. Le Gall, G. et al. Metabolomics of fecal extracts detects altered metabolic activity of gut microbiota in ulcerative colitis and irritable bowel syndrome. *J. Proteome Res.* **10**, 4208–4218 (2011).
69. Kroeze, W. K. et al. PRESTO-Tango as an open-source resource for interrogation of the druggable human GPCRome. *Nat. Struct. Mol. Biol.* **22**, 362–369 (2015).

Acknowledgements

We thank P. Helbling and M. Pavlou (Dualsystems Biotech) for their discussion regarding the LRC assay and proteomics analysis; K. Ge (National Institutes of Health, USA), J. B. Kim (Seoul National University, Korea) and O. J. Kwon (Catholic University, Korea) for providing the immortalized BACs; B. L. Roth (The University of North Carolina at Chapel Hill, USA) for providing HTLA cells; S. J. Lee (Korea University, Korea) for providing the calcium inhibitors; W. K. Huh (Seoul National University, Korea) for providing the GPCR inhibitors; J. S. Han (Seoul National University, Korea) for FPLC usage; Y. K. Oh (Seoul National University, Korea) for infrared camera usage; Y. Chung (Seoul National University, Korea) for temperature-controlled chamber usage; S. H. Yoon, L. Song, J. W. Kim and S. E. Choi (Seoul National University, Korea) for their technical assistance with the tissue sampling and preparation for FACS analysis; T. J. Ahn (KoBioLabs, Inc.) for cytokine analysis of bacterial isolates in cell lines; I. S. Cho (KoBioLabs, Inc.) for producing *EcPrc*; and the staff at the Samsung Medical Center for providing infant faecal samples. This work was supported by the National Research

Foundation of Korea (NRF) (no. NRF-2018R1A2A1A05078258). C.H.C. was supported by the Global Ph.D. Fellowship program and a NRF grant funded by the Korean government (no. NRF-2018H1A2A1061914).

Author contributions

H.S.Y., C.H.C. and G.K. contributed to the experiment design and interpreted all of the results. H.S.Y. narrowed down to the target protein using the in vitro L cell system, performed BAT-related experiments and isolated bacterial strains from infant faecal samples. C.H.C. contributed to daily administration of treatment in mouse experiments. C.H.C. performed cloning and, with assistance from M.S.Y., carried out protein expression. M.S.Y. and S.J.J. provided technical assistance with tissue sampling. S.J.J. performed QIIME II with correlation analysis and the GLP-1R β -arrestin assay. H.J.Y. participated in discussions and provided all of the assistance. J.-h.K. performed a single injection of P9 in mice and analysed systemic GLP-1. D.H. performed the proteomic analysis. Metabolomic analysis and isolation of the *A. muciniphila* strain, with assistance from K.H.C., and the culture conditions of *A. muciniphila* were optimized by S.H.M.; T.-W.N. and K.L. performed the FPLC analysis. S.-J.L. and Y.-J.K. performed the metabolic chamber analysis. H.S.Y. wrote the manuscript with C.H.C. and edited the manuscript. All of the authors discussed the results and approved the final text of the manuscript.

Competing interests

G.K. is a founder of KoBioLabs Inc., a company that aims to characterize the role of host–microbiome interactions in chronic diseases. The other authors declare no competing interests.

Additional information

Extended data is available for this paper at <https://doi.org/10.1038/s41564-021-00880-5>.

Supplementary information The online version contains supplementary material available at <https://doi.org/10.1038/s41564-021-00880-5>.

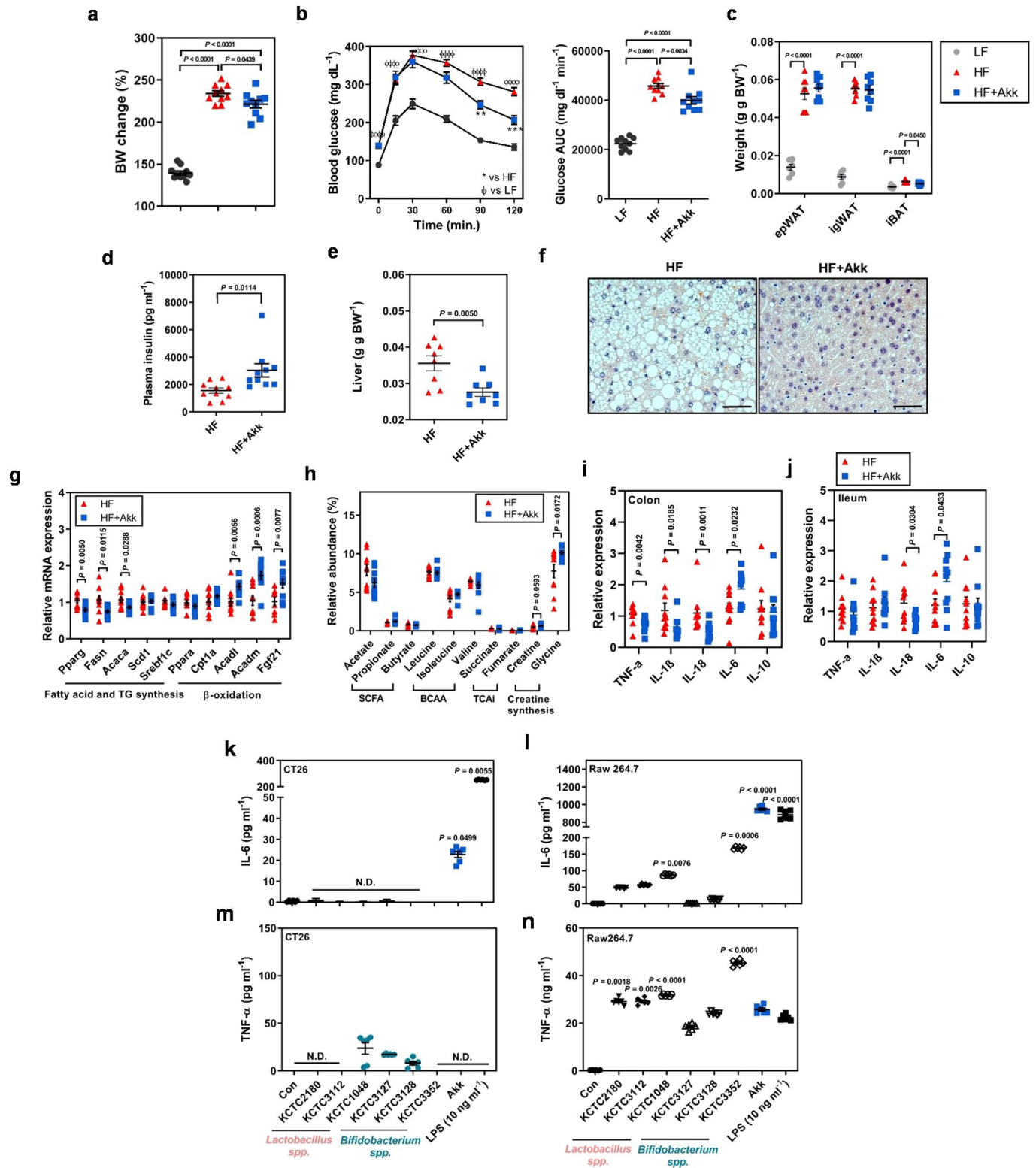
Correspondence and requests for materials should be addressed to G.K.

Peer review information *Nature Microbiology* thanks Marc Donath, Lesley Hoyles and Liping Zhao for their contribution to the peer review of this work. Peer reviewer reports are available.

Reprints and permissions information is available at www.nature.com/reprints.

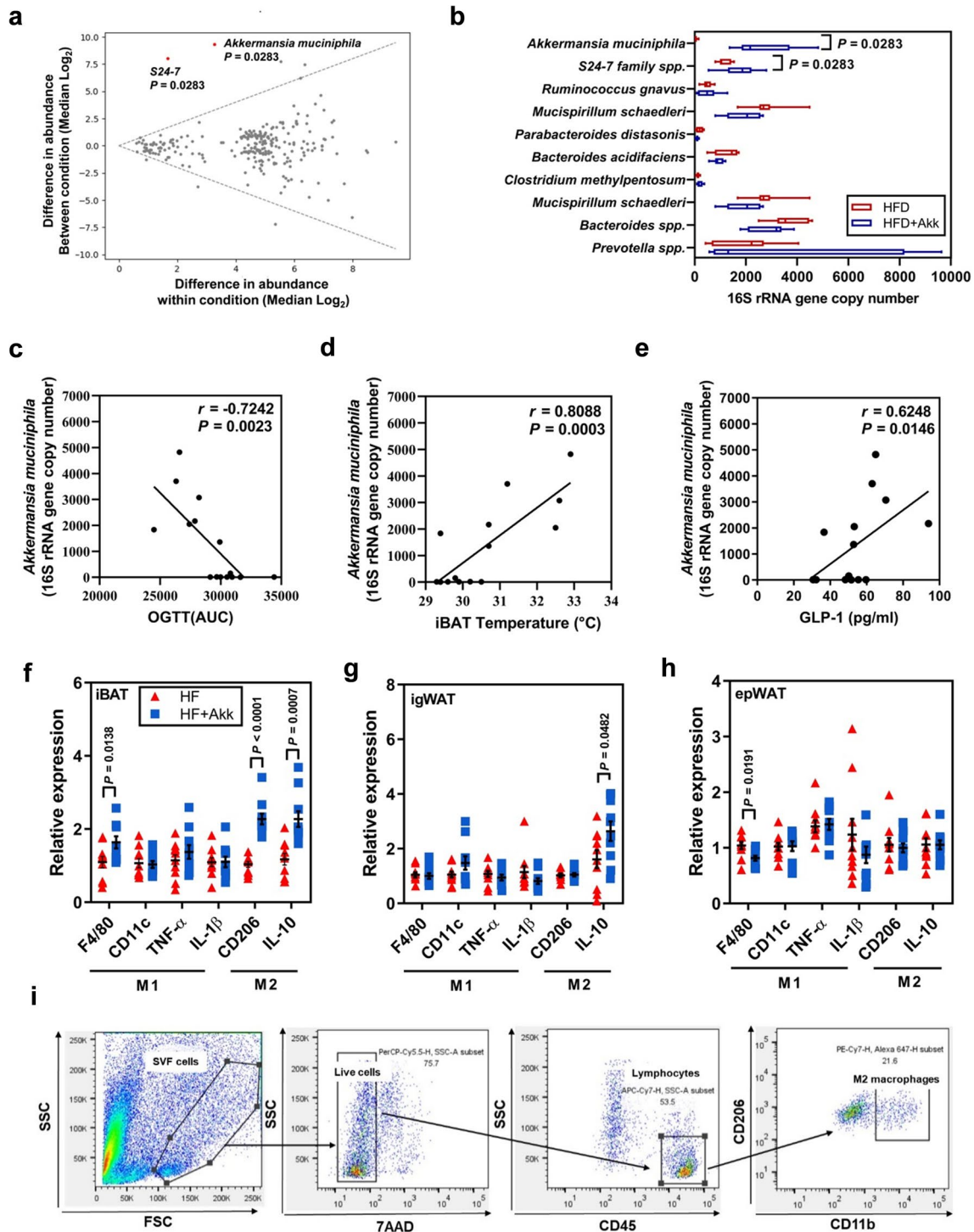
Publisher's note Springer Nature remains neutral with regard to jurisdictional claims in published maps and institutional affiliations.

© The Author(s), under exclusive licence to Springer Nature Limited 2021

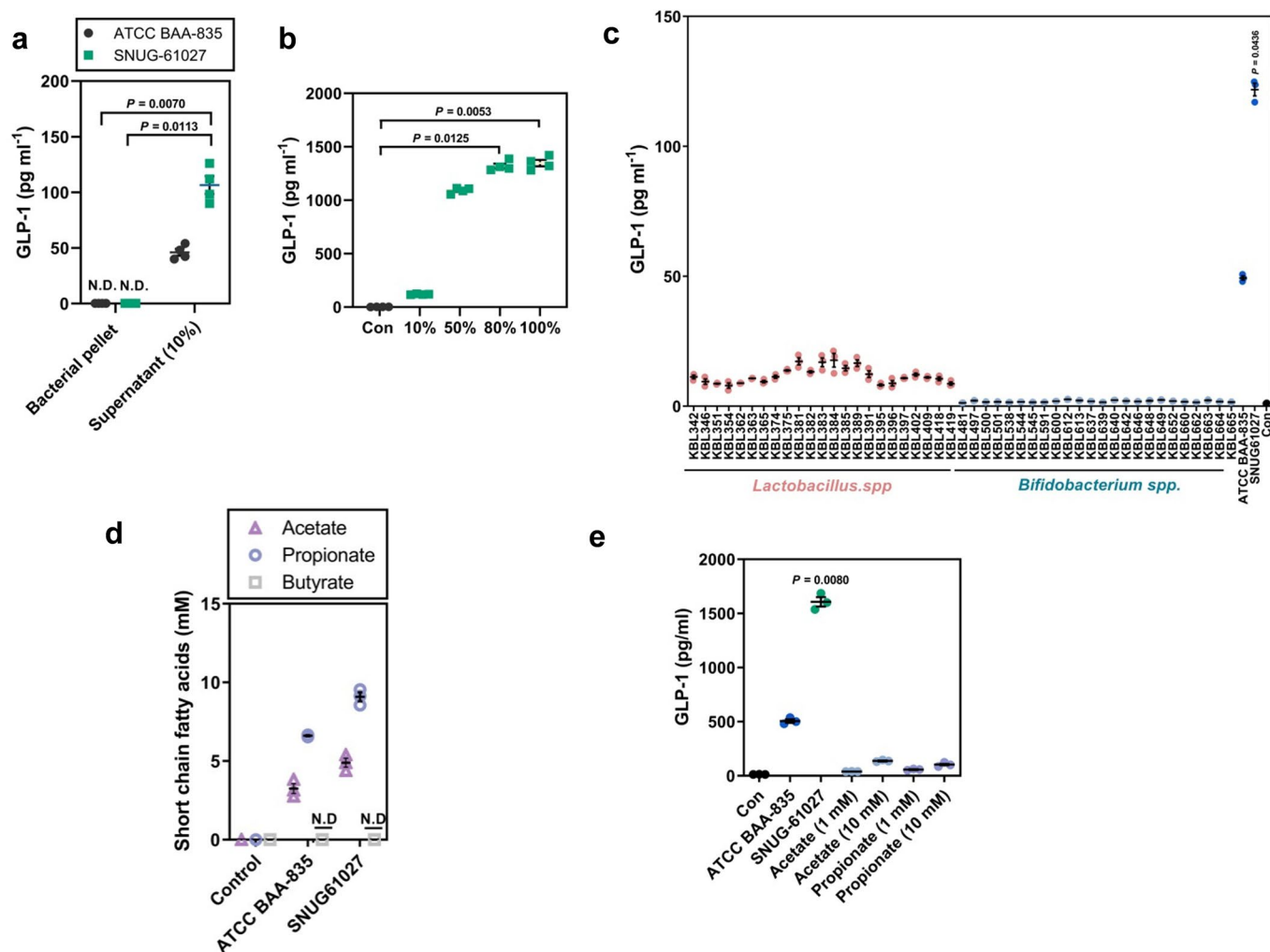


Extended Data Fig. 1 | See next page for caption.

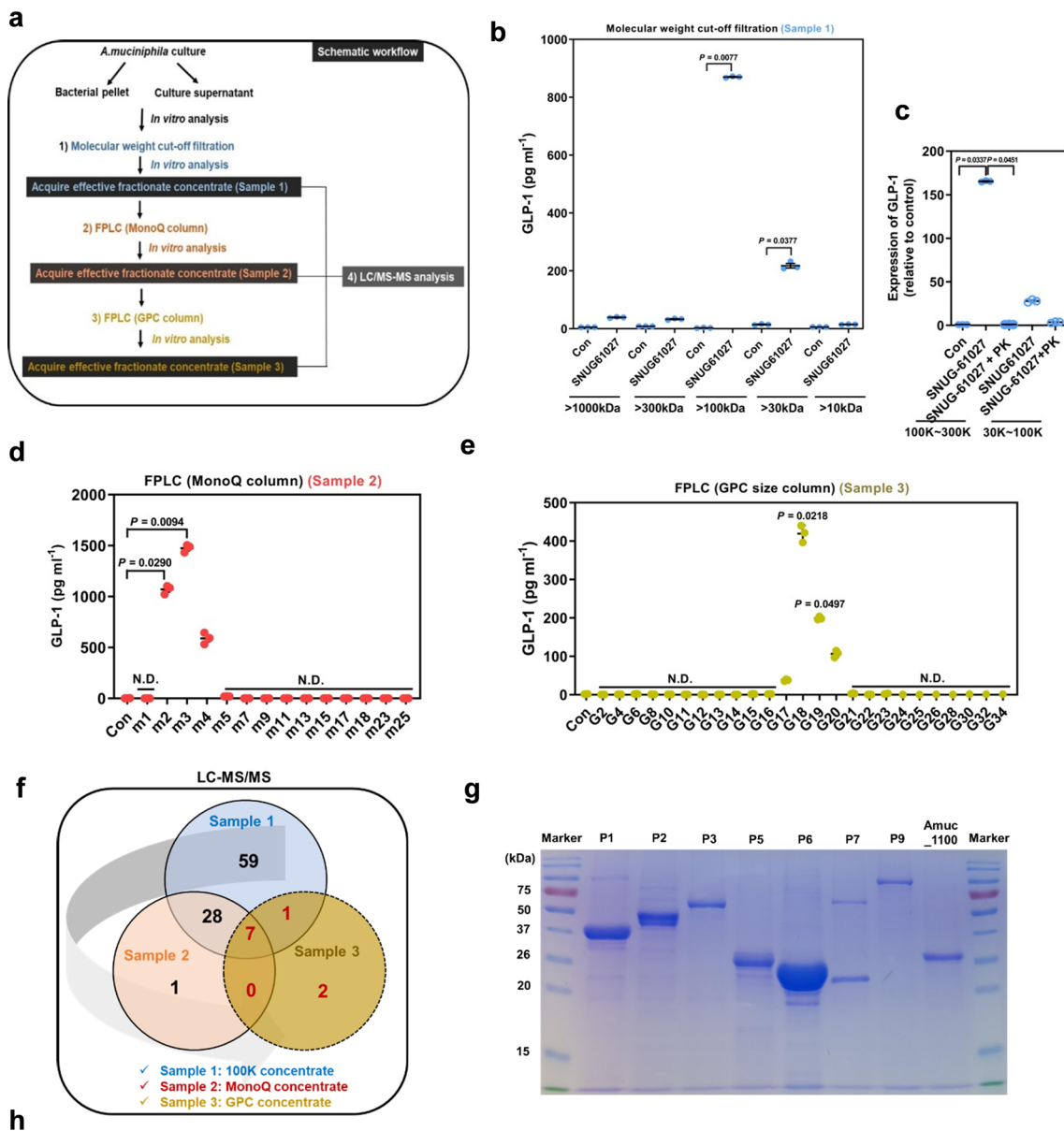
Extended Data Fig. 1 | Effects of administration of viable *A. muciniphila* for 14 weeks on insulin tolerance, adipocyte size, liver steatosis markers and intestinal cytokines levels as well as immune profiling of *A. muciniphila* effects on macrophage and colon cells. **a**, Body mass after administration of a low-fat (LF), high-fat (HF), or a high-fat diet supplemented with *A. muciniphila* (HF + Akk). **b**, Intraperitoneal glucose tolerance testing (IPGTT) data are presented in dot plots and as the areas under the curves (AUCs). **c**, Fat mass (g g body weight (BW)⁻¹), **d**, plasma insulin concentration, **e**, liver mass (g g BW⁻¹), and **f**, H&E staining of liver sections (Scale bar = 100 μ m, n = 3 mice per group). **g**, mRNA expression of fatty acid and β -oxidation genes in liver. **h**, Relative abundance of cecal metabolites, including short-chain fatty acids (SCFA), branched-chain amino acids (BCAA), tricarboxylic acid intermediates (TCAi), and metabolites involved in creatine synthesis, quantified by nuclear magnetic resonance (NMR). mRNA expression of cytokines in **(i)** colon and **(j)** ileum in HF and HF + Akk group. IL-6 secretion was measured after the stimulation of **k**, CT26 and **l**, Raw264.7 cell lines with *Lactobacillus spp.*, *Bifidobacterium spp.*, or *Akk* (ATCC BAA-835) (cell to bacteria: 1:10). TNF- α expression in response to *Akk*, *Lactobacillus spp.*, and *Bifidobacterium spp* in **m**, CT26 cell lines and **n**, Raw 264.7 cell lines. The experiment was repeated twice. *E. coli* lipopolysaccharide (LPS) was used as a positive control. Data are presented as the means \pm SEMs. Number of mice per group for **a-b**: LF: 10, HF: 10, HF + Akk: 10. Number of mice per group for **c**: LF: 6, HF: 10, HF + Akk: 10. Number of mice per group for **d-e** and **g-j**: HF: 10, HF + Akk: 10. Data were analyzed using one-way ANOVA, followed by Tukey's test for **a** and **b** (right panel) and two-way ANOVA, followed by Tukey's test for **b** (left panel). For **c-e** and **g-j**, the two-tailed unpaired *t*-test was used to analyze the data. **k-n** represent the results of three independent experiments performed in duplicate and were analyzed using the Kruskal-Wallis test, followed by Dunn's post-hoc test. **, *** and **** indicate significant differences ($P < 0.01$, < 0.001 and < 0.0001 , respectively).



Extended Data Fig. 2 | The relative abundance of *A. muciniphila* correlates with iBAT temperature and GLP-1 secretion and *A. muciniphila* administration to HF-diet-fed mice increases the M2 macrophage count in adipose tissue. **a**, Differences in the relative abundance of bacterial species between the HF and HF + Akk groups are represented by ALDEx2. The differences in abundance between and within each group for individual species were analyzed. Organisms (at the OTU and nearest neighbor species levels) with significant p values are shown as pink circles (Welch's t -statistic, corrected using the Benjamini-Hochberg method). **b**, Data showing the 16S rRNA gene count in the HF and HF + Akk groups. **c–e**, Scatter plots illustrating the statistical relationship (Spearman's correlation) between the relative abundance of *A. muciniphila* and metabolic phenotypes: OGTT AUC (oral glucose tolerance test area under the curve), iBAT temp (interscapular brown adipose tissue temperature), and GLP-1 (plasma glucagon-like peptide-1 concentration). **f–h**, mRNA expression of M1 and M2 macrophage markers in iBAT, igWAT, and epiWAT. **i**, Gating strategy for detection of M2-like macrophages (CD11b⁺ CD206⁺) in iBAT of HF-fed mice. Data are presented as the means \pm SEMs. Number of mice per group for **a–h**: HF: 10, HF + Akk: 10. Data in **f–h** were analyzed using the two-tailed unpaired t -test.

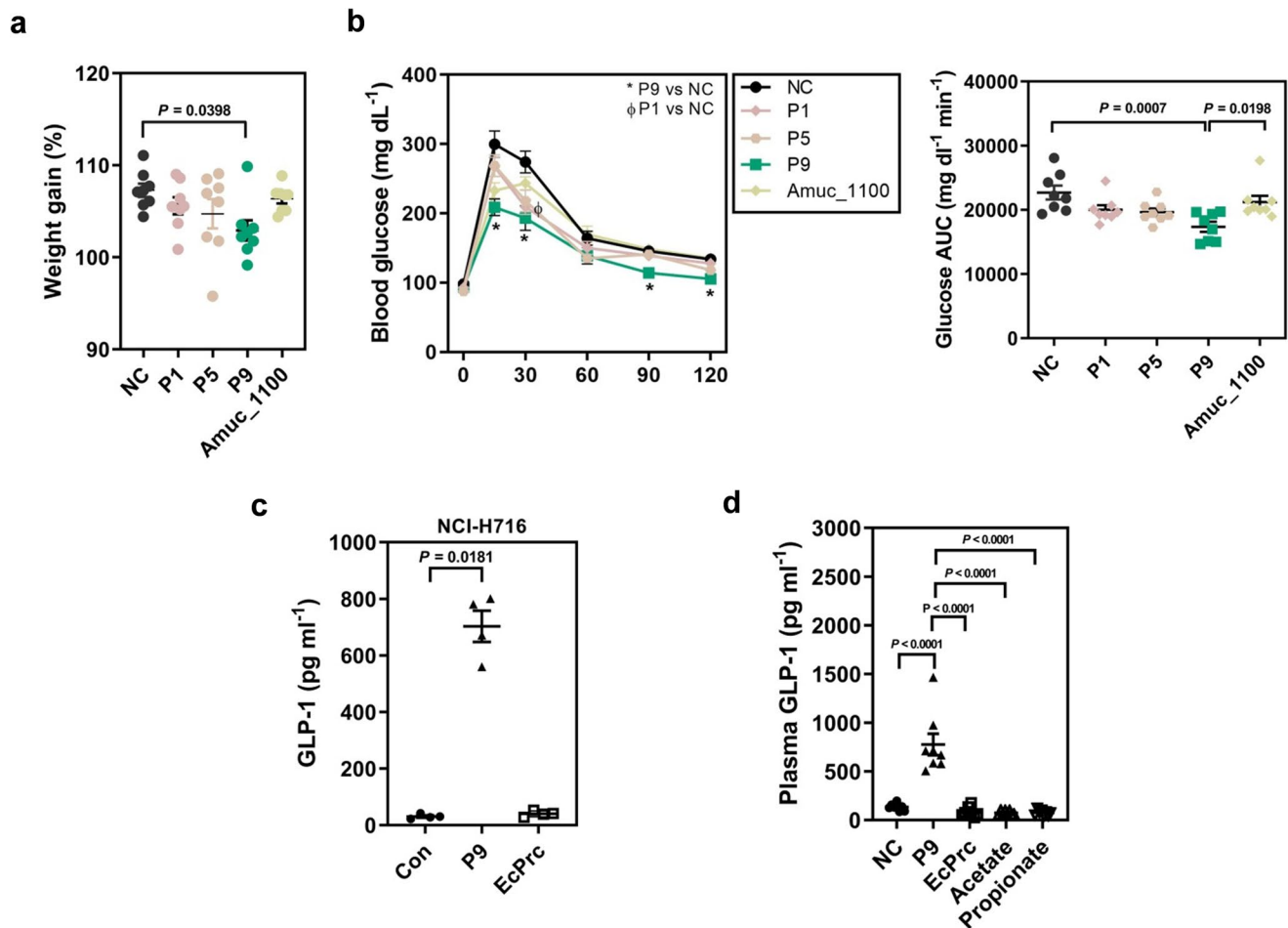


Extended Data Fig. 3 | Short-chain fatty acids produced by *A. muciniphila* are not the only factors responsible for the induction of glucagon-like peptide-1 (GLP-1). **a**, Glucagon-like peptide 1 (GLP-1) secretion after treatment of NCI-H716 cells with viable *A. muciniphila* (cell to bacteria ratio, 1:20) or cell-free supernatant (CFS) (10% v/v) (ATCC BAA-835 or SNUG-61027). **b**, GLP-1 secretion by NCI-H716 cells after treatment with various amounts of *A. muciniphila* (10–100% v/v). **c**, GLP-1 secretion after the treatment of NCI-H716 cells with CFS (10% v/v) from *A. muciniphila* (ATCC BAA-835, SNUG-61027), Korean fecal strains, *Lactobacillus spp.*, or *Bifidobacterium spp.* **d**, Short-chain fatty acids (SCFA) derived from the CFS of *A. muciniphila*, measured by GC-MS. **e**, GLP-1 secretion by NCI-H716 cells induced by the CFS of *A. muciniphila* (100% v/v), acetate (1 mM, 10 mM), or propionate (1 mM or 10 mM). Data are presented as the means \pm SEMs. The data in **a** and **b** represent the results of two independent experiments performed in duplicate. The data in **c–e** are the results of triplicate analyses. The data in **a–e** were analyzed using the Kruskal-Wallis test, followed by Dunn's *post-hoc* test. *, **, and *** indicate significant differences ($P < 0.05$, < 0.01 , and < 0.001 , respectively).

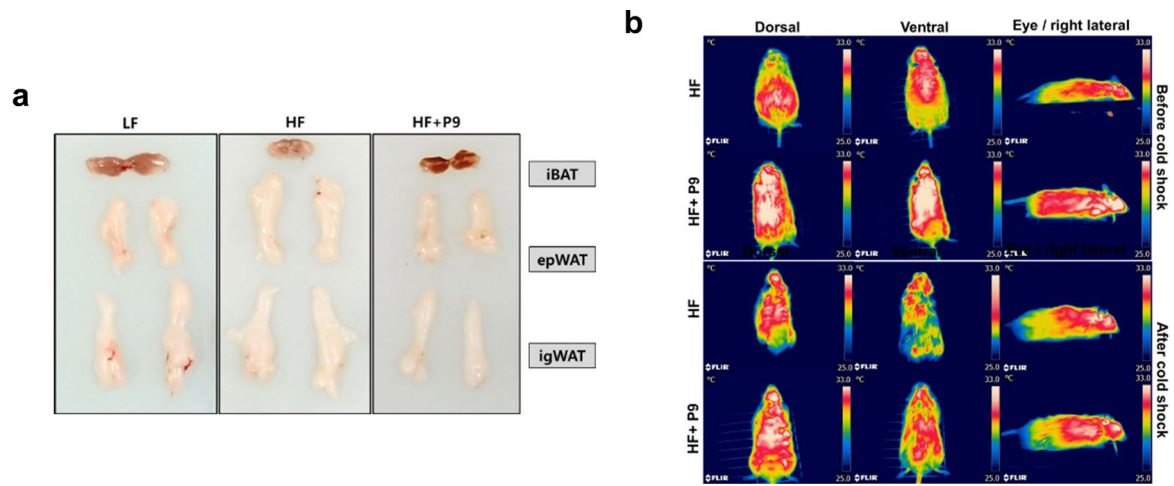


Extended Data Fig. 4 | See next page for caption.

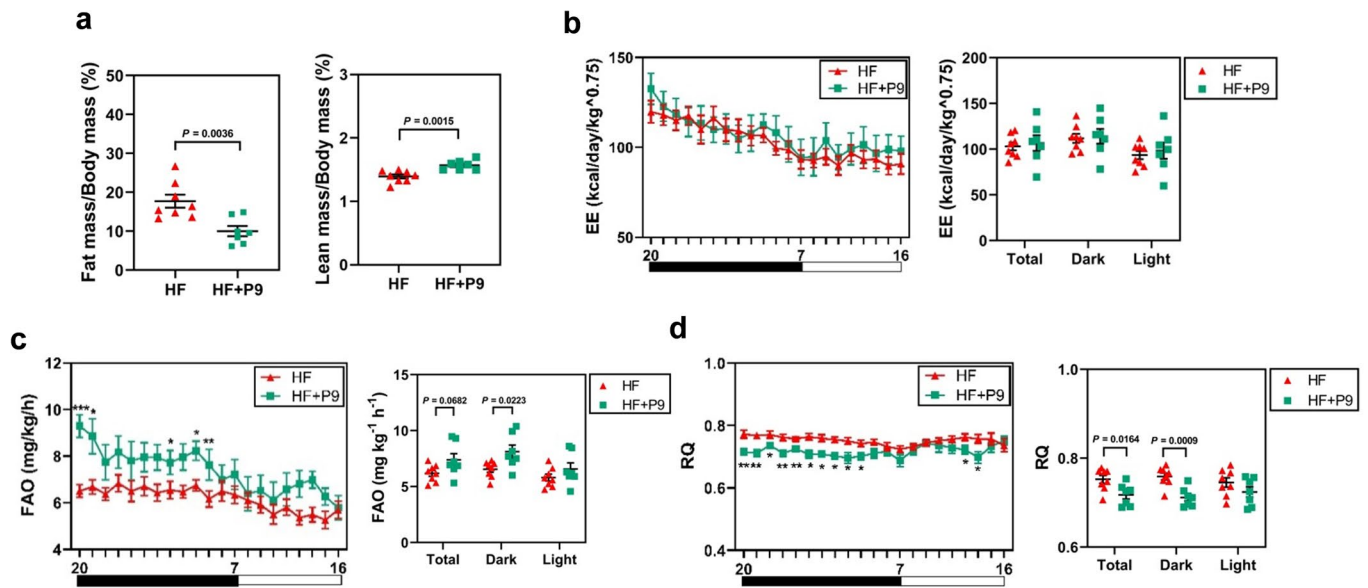
Extended Data Fig. 4 | Profiling of *A. muciniphila* supernatant fractions that induced glucagon-like peptide-1 (GLP-1) secretion. **a**, Schematic workflow used to identify GLP-1-inducing fractions derived from *A. muciniphila*. **b**, The cell-free supernatant (CFS) of *A. muciniphila* was fractionated using molecular size cut-off filters, as indicated. A volume of each fraction containing 5 mg of protein was used to treat NCI-H716 cells. **c**, 100–300 kDa filtrate and the 30–100 kDa filtrate of *A. muciniphila* were treated with proteinase K ($100 \mu\text{g ml}^{-1}$) as indicated (+PK). A control sample was used that comprised BHI broth containing 5% FBS and was treated with proteinase K. The effects of each on GLP-1 expression was then analyzed. **d**, 100 K filtrates of control media and *A. muciniphila* were separated by ion exchange fast protein liquid chromatography (FPLC) and 26 fractions (m1–m26) were obtained. Each fraction was used to treat NCI-H716 cells and GLP-1 secretion was analyzed by ELISA. **e**, Concentrates of the m2–m4 fractions of Control and SNUG-61027 were separated by size columns (to generate fractions G1–G34) using the FPLC system, then the procedures listed above were followed. **f**, Venn diagram of the identified proteins. Sample 1, Sample 2, and Sample 3 are the 100 K concentrates obtained from size cut-off filtration, concentrates from the ion exchange chromatography, and concentrates from the size-exclusion chromatography, respectively. **g**, SDS-PAGE gel of the expressed proteins were processed in parallel in the same gel. **h**, Nine proteins identified by LC-MS/MS from Sample 3. Nine candidate proteins were cloned using an *E. coli* expression system according to the protein sequences for the SNUG-61027 strain. The sequence similarity for each protein between SNUG-61027 and ATCC-BAA-835 was analyzed. Data are presented as the means \pm SEMs. The data in **b–e** represent the results of triplicate experiments and were analyzed using the Kruskal-Wallis test, followed by Dunn's *post-hoc* test.



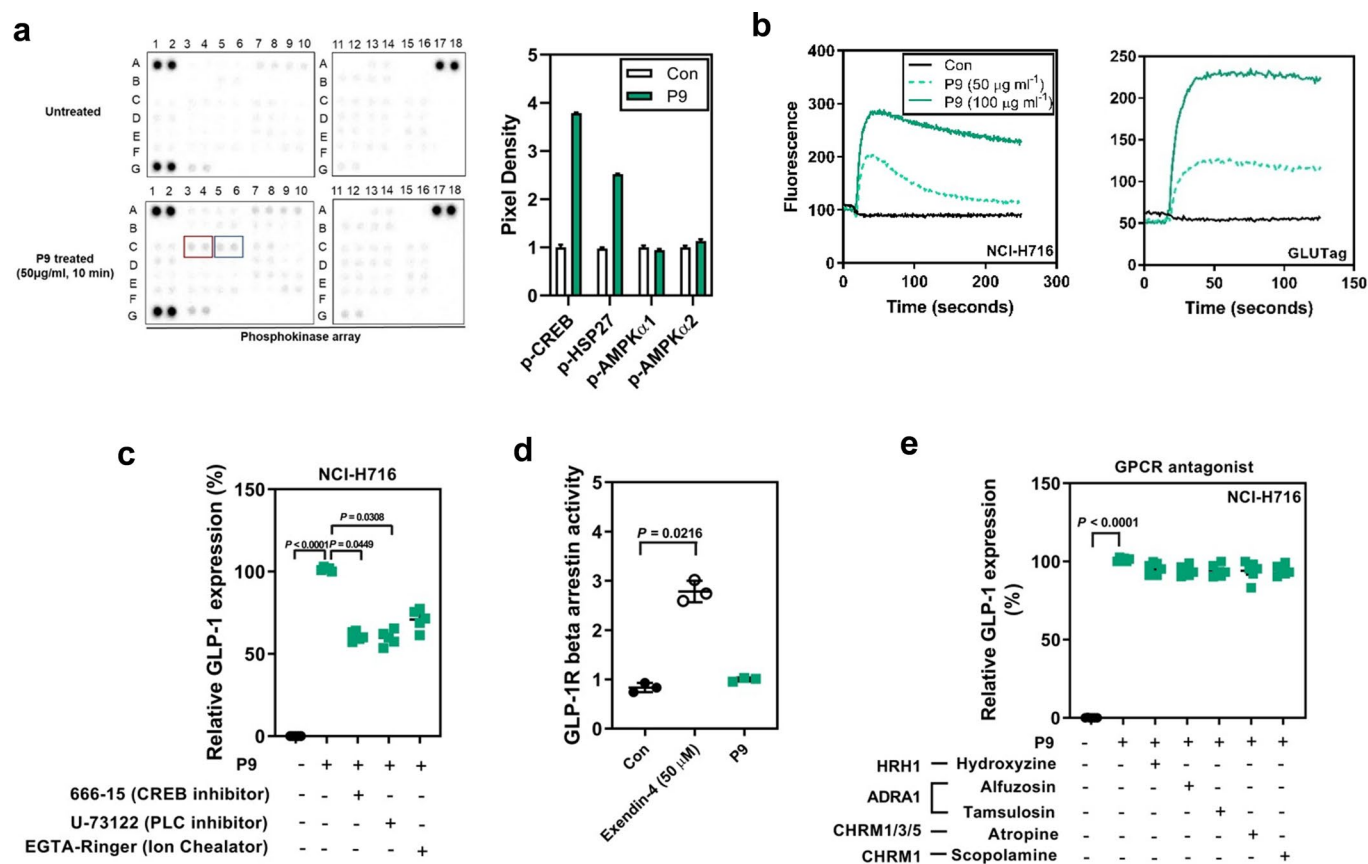
Extended Data Fig. 5 | Intraperitoneal administration of P9 improves glucose homeostasis and body mass in normal chow (NC) diet-fed mice. a, Weight gain was measured in NC-fed mice administered candidate proteins intraperitoneally (i.p.) (P1, P5, P9, or Amuc_1100) at $100 \mu\text{g}$ per mouse for 2 weeks. **b**, Oral glucose tolerance testing (OGTT) was performed and the AUCs were calculated. The data in **c** represent the effects of P9 derived from *A. muciniphila* and EcPrc (S41 family derived from *E. coli*) on GLP-1 secretion by NCI-H716 cells. **d**, Plasma GLP-1 levels were measured after the single i.p. injection ($300 \mu\text{g}$ per mouse) of each respected group. Data are presented as the means \pm SEMs. Number of mice per group for **a** and **b**: NC: 8, P1: 8, P5: 8, P9: 8, Amuc_1100: 8 and for **d**, NC: 8, EcPrc: 8, Acetate: 8, Propionate: 8. Data were analyzed using one-way ANOVA, followed by Tukey's *post-hoc* test for **a**, **d**. For **b**, data were analyzed using two-way ANOVA, followed by Tukey's *post-hoc* test. The data in **c** are the results of duplicate experiments and were analyzed using the Kruskal-Wallis test, followed by Dunn's *post-hoc* test. * or ϕ indicate significant differences, $P < 0.05$.



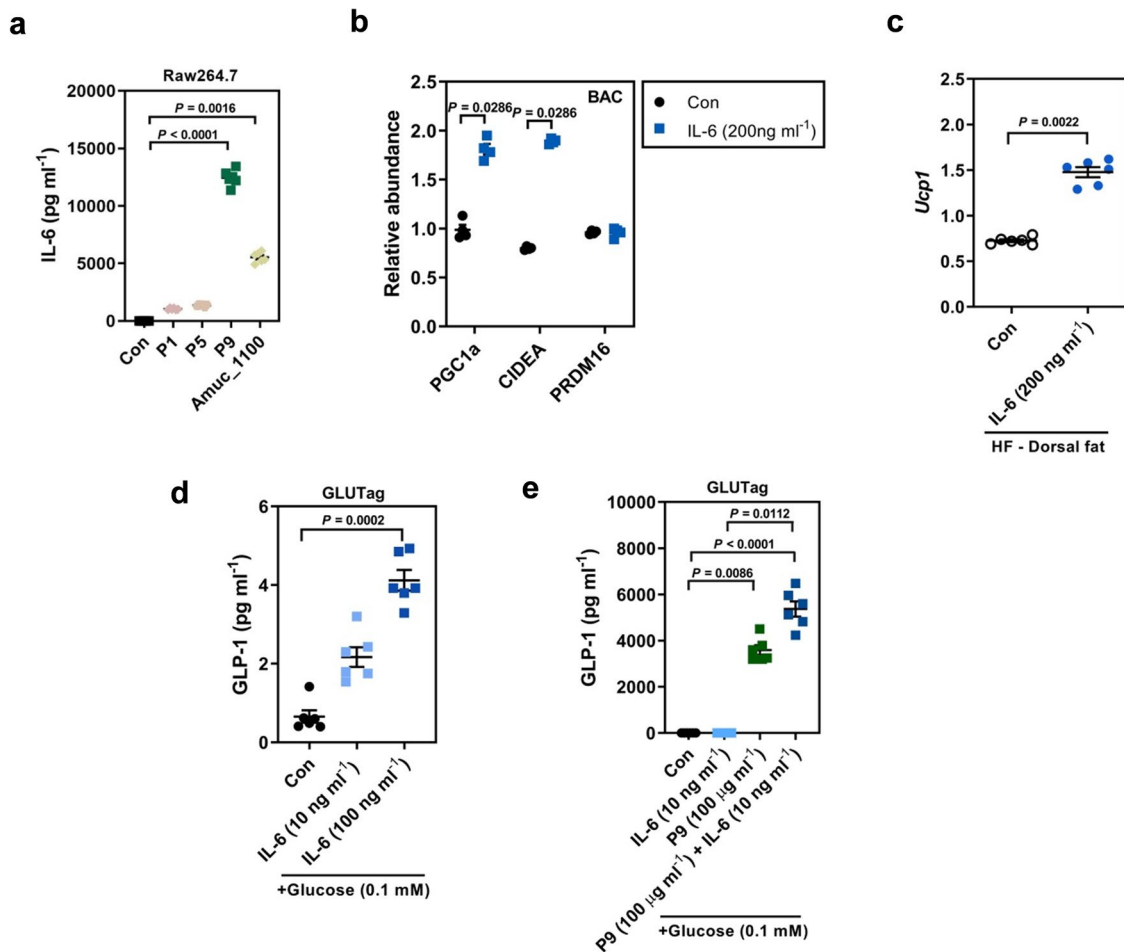
Extended Data Fig. 6 | Oral administration of P9 reduces adipose tissue mass and induces thermogenesis in high-fat diet-fed mice. a, Gross appearance of the adipose tissue depots. **b**, Representative infrared thermographic images of the temperatures of the mice are presented at room temperature (RT) (top) and after a cold shock at 5 °C for 4 h (bottom) (n=3 per group).



Extended Data Fig. 7 | Indirect calorimetry and body composition analysis following acute treatment with P9. Mice were fed a high-fat diet and were orally administered P9 protein 100 μ g or vehicle for 10 days ($n = 8$ mice per group). Oxygen consumption (VO_2), carbon dioxide production (VCO_2), respiratory quotient (RQ), and energy expenditure were calculated every 3 min using METABOLISM software (V2.2.01, Panlab-Harvard Apparatus). Fatty acid oxidation (FAO) was calculated using the following formula: $(1.6946 \times \text{VO}_2) - (1.7012 \times \text{VCO}_2)$. **a**, Body composition of the mice (% fat mass, lean mass), measured using a Minispec LF90 analyzer. **b**, Energy expenditure, **c**, FAO, and **d**, RQ. Data are presented as the means \pm SEMs. Number of mice per group: HF: 8, HF + P9: 8. Data were analyzed using the two-tailed unpaired *t*-test. *, ** and *** indicate significant differences ($P < 0.05$, < 0.01 and < 0.001 , respectively).

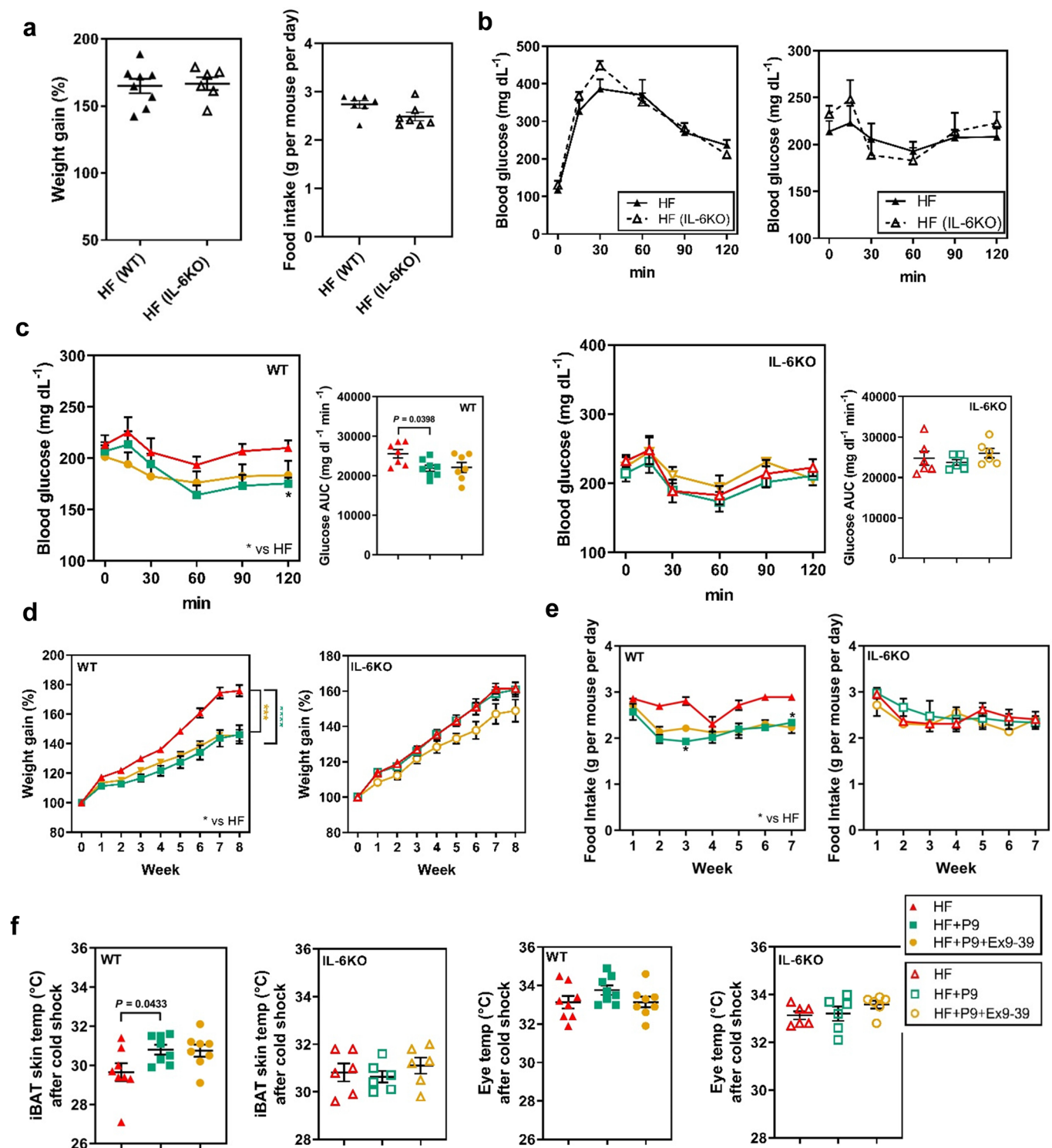


Extended Data Fig. 8 | The induction of GLP-1 secretion, by P9 involves activation of the CREB signaling pathway, but was attenuated by GPCR antagonists. **a**, Kinase phospho-profiles after P9 or vehicle treatment of NCI-H716 cells for 10 min, performed using a Proteome profile phospho-kinase array kit (Red square: p-CREB, Blue square: p-HSP27) (experiments were performed in duplicate). **b**, Ca²⁺ influx into NCI-H716 (left) and GLUTag (right) cells after treatment with 50 μ g ml⁻¹ or 100 μ g ml⁻¹ of P9 (n = 6 per group). **c**, NCI-H716 cells were treated with calcium inhibitors (10 μ M) 15 min before the P9 treatment (100 μ g ml⁻¹) for 2 h, then GLP-1 secretion was quantified (n = 6 per group). **d**, GLP-1 receptor (GLP-1R) beta-arrestin activity test data (n = 3 per group) (exendin-4: GLP-1R agonist). **e**, NCI-H716 cells were treated with GPCR antagonists (10 μ M) or vehicle (DMSO) for 15 min before P9 treatment (50 μ g ml⁻¹), then incubated for an additional 2 h, after which GLP-1 secretion was analyzed (n = 6 per group). Data are presented as the means \pm SEMs. The data in **c** and **e** represent the results of three independent experiments. The data in **a** and **c-e** were analyzed using the Kruskal-Wallis test, followed by Dunn's *post-hoc* test.



Extended Data Fig. 9 | P9 induces IL-6 secretion by macrophage cell lines and IL-6 directly regulates thermogenic gene expression in brown adipocytes.

a, IL-6 expression in Raw264.7 cells after P1, P5, or P9 treatment ($10 \mu\text{g ml}^{-1}$) overnight. **b**, Thermogenic gene expression in immortalized brown preadipocytes (BAC) and **c**, *Ucp1* gene expression in primary preadipocytes derived from interscapular brown adipose depots treated with recombinant mouse IL-6 (200 ng ml^{-1}) for 6 h. **d**, GLP-1 secretion by GLUTag cells after treatment of IL-6 in glucose condition (0.1 mM). **e**, GLP-1 secretion by GLUTag cells after treatment of IL-6 or P9 or IL-6 together with P9 in glucose condition (0.1 mM). Data are presented as the means \pm SEMs. Data were analyzed using the Kruskal-Wallis test, followed by Dunn's *post-hoc* test for **a**, **d**, and **e**; and by the Mann-Whitney test for **b** and **c**. The data represent the results of three independent experiments performed in duplicate, except in **b**, where they represent the results of two independent experiments performed in duplicate.



Extended Data Fig. 10 | P9 promotes thermogenesis via the GLP-1R signaling pathway and IL-6. **a**, Weight gain and food intake, and **b**, OGTT and ITT data after 8 weeks of HF-diet-feeding (WT: n=8, IL-6KO: n=6). **c**, Insulin tolerance testing (ITT) and AUC data for wild type (WT) and IL-6 knockout (IL-6 KO) HF-fed mice that were orally administered P9 (100 μg per mouse) ± i.p. injected with exendin 9-39 (a GLP-1R antagonist, 0.8 μg per mouse) for 8 weeks. n=8 mice per group for WT (left) and n=6 mice per group for IL-6 KO (right) mice. **d**, Weight gain, **e**, food intake (g per mouse per day), and **f**, temperatures of the iBAT and eye, measured after a cold shock at 5°C for 4 h by infrared thermography (n=8 mice per group). Data are presented as the means ± SEMs. Number of mice per group for c-e: WT HF: 7, HF + P9: 8, HF + P9 + Ex9-39: 7; IL-6 KO mice HF: 6, HF + P9: 6, HF + P9 + Ex9-39: 6. Number of mice per group for f: WT HF: 8, HF + P9: 8, HF + P9 + Ex9-39: 8; IL-6 KO mice: HF: 6, HF + P9: 6, HF + P9 + Ex9-39: 6. Data were analyzed using two-way ANOVA, followed by Tukey's *post-hoc* test for c (left panel), d, and e. For the data in c (right panel), one-way ANOVA, followed by Tukey's *post-hoc* test was used. The unpaired *t*-test was used to analyze the data in f. *, ***, and **** indicate significant differences ($P < 0.05$, < 0.001 , and < 0.0001 , respectively).

Reporting Summary

Nature Research wishes to improve the reproducibility of the work that we publish. This form provides structure for consistency and transparency in reporting. For further information on Nature Research policies, see [Authors & Referees](#) and the [Editorial Policy Checklist](#).

Statistics

For all statistical analyses, confirm that the following items are present in the figure legend, table legend, main text, or Methods section.

n/a Confirmed

- | | | |
|-------------------------------------|-------------------------------------|--|
| <input type="checkbox"/> | <input checked="" type="checkbox"/> | The exact sample size (n) for each experimental group/condition, given as a discrete number and unit of measurement |
| <input type="checkbox"/> | <input checked="" type="checkbox"/> | A statement on whether measurements were taken from distinct samples or whether the same sample was measured repeatedly |
| <input type="checkbox"/> | <input checked="" type="checkbox"/> | The statistical test(s) used AND whether they are one- or two-sided
<i>Only common tests should be described solely by name; describe more complex techniques in the Methods section.</i> |
| <input checked="" type="checkbox"/> | <input type="checkbox"/> | A description of all covariates tested |
| <input type="checkbox"/> | <input checked="" type="checkbox"/> | A description of any assumptions or corrections, such as tests of normality and adjustment for multiple comparisons |
| <input type="checkbox"/> | <input checked="" type="checkbox"/> | A full description of the statistical parameters including central tendency (e.g. means) or other basic estimates (e.g. regression coefficient) AND variation (e.g. standard deviation) or associated estimates of uncertainty (e.g. confidence intervals) |
| <input type="checkbox"/> | <input checked="" type="checkbox"/> | For null hypothesis testing, the test statistic (e.g. F , t , r) with confidence intervals, effect sizes, degrees of freedom and P value noted
<i>Give P values as exact values whenever suitable.</i> |
| <input checked="" type="checkbox"/> | <input type="checkbox"/> | For Bayesian analysis, information on the choice of priors and Markov chain Monte Carlo settings |
| <input checked="" type="checkbox"/> | <input type="checkbox"/> | For hierarchical and complex designs, identification of the appropriate level for tests and full reporting of outcomes |
| <input type="checkbox"/> | <input checked="" type="checkbox"/> | Estimates of effect sizes (e.g. Cohen's d , Pearson's r), indicating how they were calculated |

Our web collection on [statistics for biologists](#) contains articles on many of the points above.

Software and code

Policy information about [availability of computer code](#)

Data collection

Excel (Versions 16.42 and 16.43; Microsoft) was used for most data collection. Reverse transcription qPCR data was collected using an Applied Biosystems StepOnePlus PCR system using the StepOnePlus software (Version 2.1; Applied Biosystems).

Data analysis

QIIME2 software package (QIIME2 version 2020.2 ; <http://qiime.org/>), Greengenes 13.8 database, CASAVA, METABOLISM, FlowJo ver.10.4.2 software, GraphPad Prism 7.04

For manuscripts utilizing custom algorithms or software that are central to the research but not yet described in published literature, software must be made available to editors/reviewers. We strongly encourage code deposition in a community repository (e.g. GitHub). See the Nature Research [guidelines for submitting code & software](#) for further information.

Data

Policy information about [availability of data](#)

All manuscripts must include a [data availability statement](#). This statement should provide the following information, where applicable:

- Accession codes, unique identifiers, or web links for publicly available datasets
- A list of figures that have associated raw data
- A description of any restrictions on data availability

RNA sequencing data and 16S rRNA gene sequencing data that support the findings of this study have been deposited in the European Nucleotide Archive (ENA) with the accession number, PRJEB36198 for RNA sequencing addressed in Figure 3. and PRJEB36225 for 16S rRNA gene sequencing addressed in Extended Data Fig. 2. Whole genome sequencing data of SNUG-61027 is deposited in ENA under accession number, PRJEB42664 and publicly available.

Field-specific reporting

Please select the one below that is the best fit for your research. If you are not sure, read the appropriate sections before making your selection.

Life sciences Behavioural & social sciences Ecological, evolutionary & environmental sciences

For a reference copy of the document with all sections, see [nature.com/documents/nr-reporting-summary-flat.pdf](https://www.nature.com/documents/nr-reporting-summary-flat.pdf)

Life sciences study design

All studies must disclose on these points even when the disclosure is negative.

Sample size	Most of the obese mice experiments, 8 mice are used. Also the availability of animal facility limited us to do 8 mice per group. Although, for the knockout mice we did 6 mice per group due to the availability of the facility and capacity of the in-house breeding mice.
Data exclusions	We did not exclude or include any data to the experiment.
Replication	All the results in the manuscripts were repeated more than two times and was all replicated.
Randomization	We randomized the mice group to have the same average starting weight group as close as possible. Also other samples were randomly sorted into experimental groups.
Blinding	Our investigators were not blinded to group allocation for data collection and analysis for any experiment performed in this study due to size of the research group. All the mice used in this experiment was handled mostly by a single investigator. Because of this issue, we did not have additional personal that was required for blinding.

Reporting for specific materials, systems and methods

We require information from authors about some types of materials, experimental systems and methods used in many studies. Here, indicate whether each material, system or method listed is relevant to your study. If you are not sure if a list item applies to your research, read the appropriate section before selecting a response.

Materials & experimental systems

n/a	Involved in the study
<input type="checkbox"/>	<input checked="" type="checkbox"/> Antibodies
<input type="checkbox"/>	<input checked="" type="checkbox"/> Eukaryotic cell lines
<input checked="" type="checkbox"/>	<input type="checkbox"/> Palaeontology
<input type="checkbox"/>	<input checked="" type="checkbox"/> Animals and other organisms
<input type="checkbox"/>	<input checked="" type="checkbox"/> Human research participants
<input checked="" type="checkbox"/>	<input type="checkbox"/> Clinical data

Methods

n/a	Involved in the study
<input checked="" type="checkbox"/>	<input type="checkbox"/> ChIP-seq
<input type="checkbox"/>	<input checked="" type="checkbox"/> Flow cytometry
<input checked="" type="checkbox"/>	<input type="checkbox"/> MRI-based neuroimaging

Antibodies

Antibodies used	ICAM-2 blocking peptide (#MBS823225) (MyBioSource Inc., San Diego, CA), anti-ICAM-2 (BD Pharmigen, 3C4 (mIC2/4) (#BD553326) (BD Bioscience San Jose, CA), anti-total KTN1 antibody (#A44072) (Antibodies Solutions, Cambridge, UK), mouse anti- β tubulin [Thermo Fisher Scientific], CD45-APC-Cy7 (#BD557659), CD11b-PE-Cy7 (#BD561098), and CD206-Alexa Fluor 647 (#BD565250)
Validation	<ol style="list-style-type: none"> ICAM-2 blocking peptide (#MBS823225) (MyBioSource Inc., San Diego, CA) Host: Synthetic Species Reactivity: Human, Mouse, Rat Application: Blocking (BL) The peptide is used to block Anti-CD102 Antibody reactivity. https://www.mybiosource.com/icam2-human-mouse-rat-blocking-peptide/cd102/823225 anti-ICAM-2 (BD Pharmigen, 3C4 (mIC2/4) (#553326) (BD Bioscience San Jose, CA) Purified Rat Anti-Mouse CD102 Host: Rat Type: Primary Monoclonal (Clone 3C4 (mIC2/4)) Application: Blocking experiments, Flow cytometry, Immunohistochemistry (IHC), Immunoprecipitation (IP). https://www.citeab.com/antibodies/2408256-553326-purified-rat-anti-mouse-cd102 anti-total KTN1 antibody (#A44072) (Antibodies Solutions, Cambridge, UK)

Host: Rabbit
 Reactivity: Human
 Clonality: Polyclonal
 Applications: Western Blot
<https://www.antibodies.com/ktn1-antibody-a44072>

4. mouse anti- β tubulin (#32-2600) [Thermo Fisher Scientific]
 Host: Mouse
 Reactivity: Dog, C. elegans, Human, Mouse, Non-human primate, Rat
 Clonality: Monoclonal
 Applications: Western Blot and Blocking experiments
<https://www.thermofisher.com/antibody/product/beta-Tubulin-Antibody-clone-2-28-33-Monoclonal/32-2600>
5. APC-Cy™7 Rat Anti-Mouse CD45 (BD Bioscience San Jose, CA)
 Host: Rat
 Reactivity: Mouse
 Clonality: Monoclonal
 Applications: Flow cytometry
<https://www.bdbiosciences.com/eu/applications/research/stem-cell-research/cancer-research/mouse/apc-cy7-rat-anti-mouse-cd45-30-f11/p/557659>
6. PE-Cy™7 Rat Anti-CD11b (BD Bioscience San Jose, CA)
 Host: Rat
 Reactivity: Mouse
 Clonality: Monoclonal
 Applications: Flow cytometry
<https://www.bdbiosciences.com/us/applications/research/stem-cell-research/mesenchymal-stem-cell-markers-bone-marrow/mouse/negative-markers/pe-cy7-rat-anti-cd11b-m170/p/561098>
7. Alexa Fluor® 647 Rat Anti-Mouse CD206 (BD Bioscience San Jose, CA)
 Host: Rat
 Reactivity: Mouse
 Clonality: Monoclonal
 Applications: Flow cytometry
<https://www.bdbiosciences.com/us/reagents/research/antibodies-buffers/immunology-reagents/anti-human-antibodies/cell-surface-antigens/alex-fluor-647-rat-anti-mouse-cd206-mr5d3/p/565250>

Eukaryotic cell lines

Policy information about [cell lines](#)

Cell line source(s)	NCI-H716 human intestinal cell line (ATCC® CCL-251™) HEK293 human embryonic kidney [HEK-293] (ATCC® CRL-1573) GLUTag cell line was provided by Dr. D. J. Drucker (University of Toronto, Toronto, Canada) Raw 264.7 (Korean Cell Line Bank) Primary human intestine epithelial cells (InEpC) (CC-2931) Immortalized brown preadipocytes were provided by Dr. Kai Ge (NIDDK, NIH, Bethesda, MD)
Authentication	Cells were authenticated by morphological appearance and growth characteristics.
Mycoplasma contamination	All cell lines used in this manuscripts were negative in mycoplasma contamination test.
Commonly misidentified lines (See ICLAC register)	The immortalized brown preadipocytes cell line was created in Kai Ge's lab (NIDDK, NIH, Bethesda, MD) and we have data in this manuscript (Extended Data Fig.9b). This was necessary because we needed to understand the brown preadipocyte cell and its response to IL-6. The reference (PMID: 27777310) of this cell line is provided in the manuscript.

Animals and other organisms

Policy information about [studies involving animals](#); [ARRIVE guidelines](#) recommended for reporting animal research

Laboratory animals	The mouse we used in manuscript were C57BL/6J strain, male and mostly 8 weeks in age.
Wild animals	The study did not involve wild animals.
Field-collected samples	The study did not involve samples from the Field.
Ethics oversight	The animals were reviewed and approved by the Institutional Animal Care and Usage Committee (IACUC) of Seoul National University.

Note that full information on the approval of the study protocol must also be provided in the manuscript.

Human research participants

Policy information about [studies involving human research participants](#)

Population characteristics	The human subjects provided their fecal samples for research reasons the age of the participants were under 4 months in age. The participants was n=20 in total and the gender was 7 males and 13 females. The weight was 2.7-4.0 kg and had no disease status.
Recruitment	The participants were randomly selected that were under 4 months of age. The fecal sample was collected from each human participant.
Ethics oversight	All experiments were performed in accordance with the relevant guidelines and regulations and were approved by the Institutional Review Board of Seoul National University (IRB No 1405/002-008) and Samsung Medical Center (SMC 2014-11-023-001).

Note that full information on the approval of the study protocol must also be provided in the manuscript.

Flow Cytometry

Plots

Confirm that:

- The axis labels state the marker and fluorochrome used (e.g. CD4-FITC).
- The axis scales are clearly visible. Include numbers along axes only for bottom left plot of group (a 'group' is an analysis of identical markers).
- All plots are contour plots with outliers or pseudocolor plots.
- A numerical value for number of cells or percentage (with statistics) is provided.

Methodology

Sample preparation	To isolate adipocytes from the iBAT of each mouse (n = 8/group), the interscapular adipose tissue was dissected, minced finely with scissors, and digested in HBSS buffer containing collagenase (1 mg/ml collagenase type II, 0.5 % BSA) at 37 °C for 30 min. The cells were then passed through a 100 µm cell strainer and washed twice with PBS, and the RBCs were lysed. The cells were then washed with cold PBS and incubated with staining cocktail (CD45-APC-Cy7 (#BD557659), 7AAD-PercP-Cy5.5 (#BD559925), CD11b-PE-Cy7 (#BD561098), and CD206-Alexa Fluor 647 (#565250) (BD; BD Bioscience) in FACS buffer (2 % FBS in PBS) for 20 min on ice in the dark. The cells were then washed and analyzed using a FACS Verse flow cytometer (BD Bioscience). The Flow cytometry data were analyzed using FlowJo ver.10.4.2 software. All the data were primarily gated for CD45+, 7AAD-.
Instrument	FACS Verse flow cytometer (BD Bioscience)
Software	FlowJo version 10.4.2 (BD Bioscience) was used to analyze the data.
Cell population abundance	CD45+, 7AAD- populations were counted until 10,000 cells to analyze further population.
Gating strategy	Cells were gated for CD45 positive cells then for live cells, 7AAD negative populations were gated. CD11b positive, CD206 positive populations were gated for final analysis. The gating strategy is showed in Extended data fig 2i.

Tick this box to confirm that a figure exemplifying the gating strategy is provided in the Supplementary Information.